Transportation Research Part C 178 (2025) 105220

Contents lists available at ScienceDirect

Transportation Research Part C

journal homepage: www.elsevier.com/locate/trc

# A traffic-flow-dependent macroscopic model of electric vehicle energy consumption

Marcello Montanino [a,*], Ilaria Natale [a], Chiara Fiori [b], Vincenzo Punzo [a]

[a] Department of Civil, Environmental and Architectural Engineering, Università degli Studi di Napoli Federico II, Napoli, Italy
[b] Department of Civil Engineering, Università degli Studi di Salerno, Fisciano, Italy

ARTICLE INFO

*Keywords:*
Electric vehicle energy consumption
Energy consumption rate
Vehicle acceleration
Traffic conditions
Electric vehicle routing problem
Charging location problem
Green logistics

ABSTRACT

This paper shows that the assumption of a constant link speed in macroscopic energy consumption modelling of electric vehicles (EV) – common in many applications – leads to a significant underestimation of consumptions. To address this issue, a macroscopic model that accounts for the impact of traffic dynamics on EV energy consumption is developed. Model development follows an analytical investigation which demonstrates a dependency between energy consumption and acceleration variance. Such dependency is quantified by means of a large Monte Carlo simulation experiment, in which all modelling inputs including profiles of vehicle speed and road slope are generated by means of ad hoc algorithms to resemble real-world variability. A subsequent global sensitivity analysis quantifies the contribution of each model input factor – parameters and input profiles – to the accuracy of energy consumption calculations. Results confirm that the acceleration variance is by far the most influential model input, so that model accuracy is severely compromised if driving/traffic dynamics are neglected. The proposed macroscopic energy consumption model accounts for traffic dynamics by using the vehicle speed variance as explanatory variable, being it a convenient proxy of the (hardly measurable) acceleration variance. Indeed, we show that the speed variance of vehicles in a traffic stream can be expressed as a function of measurable traffic characteristics such as traffic link density and flow. Results of the model validation against laboratory and experimental data show that the proposed traffic-flow-dependent model consistently outperforms the base macroscopic model.

## 1. Introduction

### 1.1. Background and motivation

Accurate modelling of electric vehicle (EV) energy consumption is essential to develop electric mobility. It underpins critical problems such as the design and real-time operation of e-mobility services (see literature on electric dial-a-ride, vehicle routing and scheduling problems, e.g., Schneider et al., 2014; Demir et al., 2014; Ho et al., 2018; Zhang et al., 2018; Basso et al., 2019; Sayarshad et al., 2020), the optimization of electric grid and charging infrastructure (e.g., Dong et al., 2014; He et al., 2015; Bi et al., 2018; Esmaeilnejad et al., 2023; Wang et al., 2023), and the simulation-based large-scale assessment of energy consumption (e.g., Patella

* Corresponding author.
*E-mail addresses:* marcello.montanino@unina.it (M. Montanino), ilaria.natale@unina.it (I. Natale), cfiori@unisa.it (C. Fiori), vincenzo.punzo@unina.it (V. Punzo).

https://doi.org/10.1016/j.trc.2025.105220
Received 19 November 2024; Received in revised form 28 May 2025; Accepted 2 June 2025
Available online 9 June 2025
0968-090X/© 2025 The Author(s). Published by Elsevier Ltd. This is an open access article under the CC BY license (http://creativecommons.org/licenses/by/4.0/).

et al., 2019; Zhuge et al., 2019; Yousefi et al., 2024; Rakha et al., 2025). In the context of e-mobility services, for example, accurate prediction of energy consumption is needed to design routes and charging plans. Either a consumption underestimation or overestimation would cause disruption in the service and non-optimal charging operations, indeed.

Accurate prediction of vehicle energy consumption can be achieved by using *microscopic* models fed with high-resolution vehicle trajectory data. As such data are often unavailable at the required scale for many of the mentioned applications, they can be generated through traffic micro-simulation. However, the reliance on such approach significantly increases computational complexity, often rendering problem-solving – such as in vehicle routing – computationally prohibitive. Consequently, *macroscopic* energy consumption models are commonly adopted as a more computationally efficient alternative for estimating vehicle energy consumption. These models return the vehicle energy consumption on each network segment as a function of *average* inputs, such as average speed or road slope on a segment (e.g., see review in Othman et al., 2019). Average input values depend on the level of data segregation (Li et al., 2017; Zhang et al., 2020) and are computed through a time-based or a distance-based snipping method.[1]

Three macroscopic modelling approaches to simulate energy consumption have been adopted so far in the literature. In a first approach – by far the most widely used – the energy consumption rate per unit distance travelled by a vehicle (or equivalently per unit time spent) is assumed constant over the entire network. In other approaches, data-driven models or simplified microscopic power-based models are adopted to predict an average vehicle consumption on a segment.

All the proposed approaches suffer from significant limitations that may ultimately jeopardise the accuracy of predictions. A detailed review of the available approaches is presented in Section 2. If the first approach is unable to adequately describe the variability of consumption across the network, the others lack transferability to different case studies, and suffer from potential bias in consumption prediction due to overly simplistic and unrealistic assumptions.

In particular, the *constant link speed assumption* – customarily adopted in most of the applications of the last two approaches – compromises the prediction accuracy, as it implies neglecting driving dynamics, i.e., the acceleration and deceleration transients.

This issue was acknowledged by some studies in the electric vehicle routing problem literature (e.g. Goeke and Schneider, 2015; Gallet et al., 2018; Masmoudi et al., 2018; Qi et al., 2018; Basso et al., 2019). Proposed remedies to this limiting assumption are not satisfactory, however (see Section 2). Overall, it is unclear how much the constant link speed assumption, or its remedies, like the granularity of the link segmentation affect the accuracy of energy consumption predictions.

A more systematic approach to cope with uncertain driving dynamics and vehicle characteristics when forecasting energy consumption was presented in Pelletier et al. (2019). The proposed approach relies on the identification of so-called "worst-case" vehicle energy consumption on a segment, i.e., the highest vehicle energy consumption returned by a microscopic model once fed with the "worst-case" input values. A "worst-case" speed profile, however, is hard to be determined in practice, due the considerable degree of uncertainty affecting the speed dynamics. As a matter of fact, no method to explore the impact of speed profile variability on consumption is available.

Overall, a comprehensive quantification of the impact of input modelling uncertainties on the energy consumption predictions is generally missing in the literature. This topic was only partially addressed by Fiori et al. (2021a), who focused on the sole contribution of the uncertainty in model parameters. However, disentangling the impact on consumption of the two sources of input uncertainty, i.e., model parameters and input profiles of speed and slope is essential to guide the development of enhanced macroscopic models, and ultimately identify key inputs that determine the "worst-case" consumption.

### 1.2. Contributions

Therefore, to address limitations of current modelling approaches several contributions are provided in this work.

The first contribution is a theoretical one (Section 3). A dependency between EV energy consumptions and vehicle acceleration variance is analytically demonstrated. The analysis shows that the expected value of consumptions grows with the acceleration variance and, therefore, with traffic dynamics. This contribution is crucial as it demonstrates that the widespread assumption of a constant speed value on a link to calculate EV energy consumptions can lead to a substantial prediction bias.

The second contribution consists in a thorough quantification of the identified modelling bias due to the assumption of constant link speed (Section 4). This contribution is key to establish if such bias is negligible in practical applications or requires a major modelling improvement.

To address this research question, we have introduced several methodological advancements. In order to accurately quantify the identified bias, it was essential to account for all relevant sources of uncertainty. This consideration led us to develop a Monte Carlo uncertainty propagation framework (UA) that maps uncertainties in all inputs – including model parameters, and profiles for road slope and vehicle speed – onto the output, namely, energy consumption. Additionally, a variance-based sensitivity analysis (SA) was proposed to identify the most influential inputs affecting EV energy consumption. To ensure the UA and SA approaches are both meaningful and realistic, we devised two new algorithms capable of generating synthetic speed and road slope profiles that reflect real-world variability.

This comprehensive framework represents a significant advancement over existing methodologies, overcoming the limitations of more traditional analytical approaches – such as the one discussed in Section 3 – which are constrained by their simplifying

[1] In the former, averages are calculated on data snippets divided on a time scale with fixed intervals, e.g., average speed every minute; in the latter, data are spatially divided according to the network link segmentation, or based on fixed distance segments (e.g., average link speed, or average speed per kilometre).

assumptions.

Our final contribution is a multifaceted modelling advancement, detailed in Section 5. We first demonstrate that the variance in vehicle speed – closely related to acceleration variance – accounts for the systematic underestimation of energy consumption in the macroscopic model. This finding is particularly important, as it enables the development of an unbiased macroscopic energy consumption model, expressed in terms of readily measurable traffic characteristics. In fact, we propose and calibrate an empirical relationship between speed variance and both link density and flow, using vehicle trajectory data.

The proposed model has been validated using real-world energy consumption data sampled at 1 Hz from a fleet of electric minivans (see Section 6). The final contribution of the paper involves assessing the impact of network link segmentation on result accuracy for both the baseline macroscopic model and its enhanced version – an aspect of practical importance for real-world applications.

## 2. A critical review of available macroscopic energy consumption modelling approaches

Three macroscopic modelling approaches have been proposed so far in the literature.

In the first approach, the EV energy consumption on a network link is simply assumed to be proportional to the link length through a constant coefficient here referred to as *specific energy consumption* (SEC).[2] As the assumption of a linear relationship between energy consumption and link length is appealing from a mathematical standpoint in optimisation problems, this approach has been by far the most widely adopted in the existing literature (see e.g., Erdogan and Miller-Hooks, 2012; Felipe et al., 2014; Schneider et al. 2014; Adler and Mirchandani, 2016; Desaulniers et al., 2016; Keskin and Çatay et al., 2016; Koc and Karaoglanba et al., 2016; Wen et al., 2016; Schiffer and Walther, 2017; Wang et al., 2017; Bongiovanni et al., 2019; Hiermann et al., 2019; Esmaeilnejad et al., 2023; Lian et al., 2023; Su et al., 2023). The adoption of a constant energy consumption rate, however, is structurally unable to describe the variability of consumption over a network. This is because the coefficient is unable to incorporate the dependence of consumption on actual driving dynamics.

The second approach relies upon data-driven models based on machine learning or statistical analysis to simulate EV energy consumption (see e.g., Shankar and Marco, 2013; Yi et al., 2018; Zhang et al., 2020; Pan et al., 2023). These models combine multiple data sources, possibly including also traffic conditions by means of a measure of congestion on network links. Such measure, however, can be hard to be computed, as very detailed data are required, e.g., the average number of vehicle stops per kilometre (e.g., Shankar and Marco, 2013). Furthermore, these models require a vast amount of vehicle-specific and network-specific data for training, which hinders model transferability to different case studies.

In the third approach, the "average" EV energy consumption on a network segment is computed by means of a simplified version of a microscopic power-based model (e.g., Yao et al., 2014; Brooker et al., 2015; Wu et al., 2015; Zhang and Yao, 2015; Fiori et al., 2016; Genikomsakis and Mitrentsis, 2017; Yi and Bauer, 2017; Fiori and Marzano, 2018; Fiori et al., 2021b; Hjelkrem et al., 2021; Sagaria et al., 2021; Jiang et al., 2023; Xu et al., 2023). Microscopic models based on physical laws, such as power-based models, return consumption as a function of vehicle speed and road slope profiles, vehicle characteristics, and environmental conditions. A generalized formulation of these models is given in Eq. (1):

$$EC_{micro}(t_0, t_L) = \int_{t_0}^{t_L} P_{traction}(v(t), a(t), \theta(t), m, w, \boldsymbol{\beta})dt \tag{1}$$

where $EC_{micro}(t_0, t_L)$ is the EV energy consumption for traction on a link of length $L$ travelled in the time period $[t_0, t_L]$, with $t_0$ the entrance time and $t_L$ the exit time. $P_{traction}$ is the instantaneous power requested for traction, which is a function of the instantaneous vehicle speed $v(t)$, acceleration $a(t)$, road slope $\theta(t)$, kerb mass $m$, load $w$ (which is assumed to be constant over a link), and a vector of model parameters $\boldsymbol{\beta}$ which includes the road load coefficients, the drag coefficient, the vehicle frontal area, and the efficiencies of vehicle components/systems such as the battery, the electric motor, the driveline or the regenerative braking system. Please note that, the additional energy consumption due to auxiliary systems is neglected in Eq. (1), being independent from driving dynamics.

However, since the actual input speed profile is unknown when solving a vehicle routing problem, a *constant link speed assumption* is typically made to derive a macroscopic energy consumption model (often the average link speed is adopted, see e.g., Bektas and Laporte, 2011; Franceschetti et al., 2013; Neaimeh et al., 2013; Goeke and Schneider, 2015; Gallet et al., 2018; Masmoudi et al., 2018; Qi et al., 2018; Zhang et al., 2018; Basso et al., 2019; Pelletier et al., 2019; Lu et al., 2020; Saadon Al-Ogaili et al., 2020; Sayarshad et al., 2020; Ma et al., 2021; Avishan et al., 2023). Under this assumption, Eq. (1) becomes:

$$EC_{macro}(t_0, t_L) = \int_{t_0}^{t_L} P_{traction}(\mu_v, \mu_a, \mu_\theta, m, w, \boldsymbol{\beta})dt \tag{2}$$

where $\mu_v$ is the average link speed, $\mu_a$ is the average acceleration (usually assumed to be zero), and $\mu_\theta$ is the average link slope. In other words, sophisticated models are applied in a simplified manner, i.e., ignoring acceleration, deceleration and road slope variation.

Goeke and Schneider (2015) and Masmoudi et al. (2018), acknowledged that such simplification may affect macroscopic model

[2] As the vehicle speed is assumed to be constant over a link, this is equivalent to adopt an energy consumption rate per unit travel time spent.

accuracy, and proposed to increase the link segmentation as a remedy. However, how much a constant link speed assumption, or different levels of link segmentation affect the accuracy of energy consumption predictions, remains unknown. A theoretical answer to this question is then provided in Section 3, and numerically verified in Section 4.

An alternative approach to incorporate consumption variability in a macroscopic model was proposed by Gallet et al. (2018) and Basso et al. (2019). In these works, the variability of consumption due to speed transitions at nodes (intersections and traffic lights) or bus stops, was described by a kinematic model with constant acceleration and deceleration rates. Conversely, the variability of consumptions on running links, due to stop-and-go traffic dynamics, for instance, was not considered therein.

An approach which aims to describe the consumption variability on running links via a macroscopic model was proposed by Qi et al. (2018). By noting that the EV energy consumption depends on the cumulative variations of kinetic energy between the beginning and the end of a link, polynomial functions of the average speed (differentiated by positive and negative kinetic energy) were fitted to high-resolution vehicle data segregated at the level of network links. The proposed macroscopic model resulted from the sum of such polynomial functions. The model was derived by assuming speed-independent rolling resistances and neglecting aerodynamic resistances (which is realistic only at low-speeds). Nevertheless, the influence of link length on model accuracy remains unknown. In addition, the fitted polynomials were vehicle-specific, which limits their applicability to different case studies.

A more comprehensive approach to deal with uncertain driving dynamics and vehicle characteristics, when forecasting energy consumption in an electric vehicle routing problem, was presented by Pelletier et al. (2019). To design a set of optimal vehicle routes that is robust against the variability of vehicle dynamics and performances (e.g., due to uncertain traffic conditions, weather conditions, or road surface), an optimization model with a constraint that depends on the so-called "worst-case" vehicle energy consumption on a segment was proposed. The "worst-case" consumption is obtained by microscopic model simulation with the "worst-case" input values, i.e., the model input values that produce the highest vehicle consumption among a given set of realizations.

It should be noted, however, that, if the "worst-case" values of parametric inputs, e.g., road load coefficients, drag coefficient and area, motor efficiency, are identified as soon as an analyst chooses min–max ranges of variation for those inputs, "worst-case" values for non-parametric inputs, especially the speed profile, are not easy to identify. In fact, a speed profile is the result of a combination of a multitude of factors, such as traffic conditions and driving style, infrastructure characteristics, road and weather conditions. However, no methodology was presented in Pelletier et al. (2019) to investigate the influence of speed profile variability on energy consumption (a constant link speed assumption was adopted as usual).

It is also worth mentioning that the set of "worst-case" input values may not be unique. Due to the presence of mutual interaction effects, the "worst-case" combination of model inputs does not necessarily result from the "worst-case" values of each individual input. Conversely, there may also be entirely distinct sets of input values that yield the same "worst-case" energy consumption. The latter ultimately introduces a non-negligible degree of complexity for the optimisation model.

An approach similar to Pelletier et al. (2019) to account for consumption uncertainty in electric vehicle routing optimization was presented in Jeong et al. (2024). A two-stage adaptive robust optimization model was formulated based on stochastic energy consumption rate sampled from normal or uniform distributions, also considering spatial correlation among network links. However, no (explicit) relationship between consumption distribution and traffic was outlined, making results exclusively depending on the consumption distribution assumed. Furthermore, the consumption distribution was network specific and not transferable to other networks.

Let alone these criticisms, it is unknown how much variability of simulated energy consumption can be attributed to uncertain model parameters, and how much to non-parametric inputs (primarily, the speed profile). This is deemed to be crucial to identify "worst-case" input scenarios, disregarding uninfluential inputs and focusing on the most influential ones. An answer to this question is provided in Section 4.

## 3. Analysis of the relationship between accelerations and energy consumptions

As discussed in Section 2, the approach of feeding a microscopic energy consumption model with a constant link speed profile is widely used in the literature. Despite this assumption is a convenient simplification in vehicle routing optimization problems, its impact on the accuracy of energy consumption predictions is unknown.

It is worth mentioning that Avishan et al. (2023) justified the validity of such assumption by referring to theorem 3.1 in Fontana (2013). This theorem states that, under the assumption of a regenerative braking efficiency equal to 1, the total energy consumption of an electric vehicle is only due to motion resistance. Therefore, it does not depend on the energy consumed/recovered during acceleration/braking. However, a regenerative braking efficiency equal to 1 is a naïve assumption that does not hold in practice, actually being much lower than 1, and varying with the applied deceleration rate (see Fiori et al., 2016).

The objective of this section is therefore to provide a mathematical quantification of the inaccuracy of energy consumption predictions based on the assumption of a constant link speed profile.

Let the acceleration signal $\{a_t\}$ be a stochastic process of i.i.d. zero-mean random variable $a_t$ with a variance $\sigma_a^2$, $\forall t \in \{0, 1, 2, \cdots, T\}$, where $T = \mathrm{T}/\Delta t$, T is the signal duration, and $\Delta t$ is a finite time step.

The speed signal $\{v_t\}$ results from the integral of the acceleration signal. By assuming a constant acceleration in every $\Delta t$, it yields:

$$v_t = v_{t-1} + a_t \Delta t \tag{3}$$

By assuming an initial speed value equal to $v_0$ and expanding the recurrence in Eq. (3), it yields:

$$\begin{aligned} v_1 &= v_0 + a_1 \Delta t \\ v_2 &= v_1 + a_2 \Delta t = v_0 + (a_1 + a_2)\Delta t \\ &\vdots \\ v_t &= v_{t-1} + a_t \Delta t = v_0 + \sum_{i=1}^{t} a_i \Delta t \\ &\vdots \\ v_T &= v_{T-1} + a_T \Delta t = v_0 + \sum_{i=1}^{T} a_i \Delta t \end{aligned} \tag{4}$$

Therefore, the expected value and the variance of the instantaneous speed value $v_t$ at the generic instant $t$ are:

$$\mathrm{E}[v_t] = \mathrm{E}[v_0] + \sum_{i=1}^{t} \mathrm{E}[a_i \Delta t] = v_0 \tag{5a}$$

$$\mathrm{V}[v_t] = \mathrm{V}[v_0] + \sum_{i=1}^{t} \mathrm{V}[a_i \Delta t] = \sum_{i=1}^{t} \mathrm{V}[a_i \Delta t] = t\sigma_a^2 \Delta t^2 \tag{5b}$$

Eq. (5b) shows that the variance grows with time, which is a sufficient condition for identifying a non-stationary stochastic process. Therefore, even in case of neglecting acceleration autocorrelation (as assumed here), the integration produces an autocorrelated speed signal, which is in accordance with empirical data.

In addition, Eq. (5a) shows that the expected value of speed, at each time instant, is constant and equal to the initial speed value $v_0$. Therefore, $v_0$ is the expected value of the speed over the link, which is more intuitive if $v_0$ is expressed as the ratio between the expected value of the total space travelled, $\mathrm{E}[x_T]$, and the total travel time, $T\Delta t$:

$$x_T = \sum_{i=0}^{T} v_i \Delta t = v_0 T \Delta t + \sum_{i=1}^{T} (T - i + 1) a_i \Delta t \tag{6}$$

$$\mathrm{E}[x_T]/(T\Delta t) = v_0 \tag{7}$$

According to Newton's second law of motion, the traction force applied to the vehicle wheels is made of two components: an inertial component, due to the applied acceleration signal, and a resistance component, due to motion resistances, which are customarily modelled as a quadratic function of the instantaneous speed.

The power signal results from the element-wise product of the traction force signal and the speed signal. In the following, the effect of the two components of the traction force on the power signal is studied separately. For the sake of simplicity and without loss of generality, a unit vehicle mass is assumed (in fact, the mass value simply acts as a scaling factor of the power signal).

Concerning the inertial component $\left\{P_t^{in}\right\}$, based on Eq. (4) and expanding the first three terms of the element-wise product $\{a_t\} \odot \{v_t\}$, it yields:

$$\begin{aligned} P_1^{in} &= v_0 a_1 + a_1^2 \Delta t \\ P_2^{in} &= v_1 a_2 + a_2^2 \Delta t = v_0 a_2 + \left(a_1 a_2 + a_2^2\right)\Delta t \\ P_3^{in} &= v_2 a_3 + a_3^2 \Delta t = v_0 a_3 + \left(a_1 a_3 + a_2 a_3 + a_3^2\right)\Delta t \end{aligned} \tag{8}$$

By induction:

$$P_t^{in} = v_0 a_t + \left(a_1 a_t + a_2 a_t + \cdots + a_{t-1} a_t + a_t^2\right)\Delta t = v_0 a_t + a_t \sum_{i=1}^{t} a_i \Delta t \tag{9}$$

The total energy consumption due to the *inertial component* $EC_T^{in}$ results by the integral of the power signal over time, i.e., the summation of $\left\{P_t^{in} \Delta t\right\}$:

$$EC_T^{in} = v_0 \sum_{i=1}^{T} a_i \Delta t + \sum_{i=1}^{T} a_i \sum_{j=i}^{T} a_j \Delta t^2 \tag{10}$$

Let $a$ denote the random variable at any time instant $t$. Eq. (10) becomes:

$$EC_T^{in} = v_0 T a \Delta t + 0.5 T (T+1) a^2 \Delta t^2 \tag{11}$$

Noting that a zero-mean normal distribution has odd moments equal to zero, i.e., $\mathrm{E}[a^{3i}] = 0, \forall i \in \mathbb{N}$, and even moments equal to $E[a^{2i}] = (2i-1)!!\sigma_a^{2i}, \forall i \in \mathbb{N}$, and posing $0.5T(T+1) = k$, the expected value and the variance of $EC_T^{in}$ are:

$$\mathrm{E}\left[EC_T^{in}\right] = k\mathrm{E}\left[a^2\right]\Delta t^2 = k\sigma_a^2\Delta t^2 \tag{12a}$$

$$V\left[EC_T^{in}\right] = T^2\sigma_a^2\Delta t^2 + k^2\left(\mathrm{E}\left[a^4\right] - \mathrm{E}\left[a^2\right]^2\right)\Delta t^4 = T^2\sigma_a^2\Delta t^2 + 2k^2\sigma_a^4\Delta t^4 \tag{12b}$$

Eqs. (12a-b) show that both *the expected value and the variance of the inertial component of the total consumption, $EC_T^{in}$, are a function of the acceleration variance $\sigma_a^2$.*[3] This means that the inertial component of the total consumption can be significantly affected if speed dynamics are neglected. For instance, in the NGSIM I80 (freeway) trajectory data (Punzo et al., 2011), the acceleration variance in the three datasets is, respectively, 2.79, 2.04 and 1.96 $m^2/s^4$, i.e., it decreases with the congestion increase (the average speeds of datasets are: 7.72, 6.41, 5.60 m/s). Indeed, in Eq. (12a), $\sigma_a = 0$ yields an inertial component of the consumption equal to zero:

$$\mathrm{E}\left[EC_T^{in}\right]_{\sigma_a=0} = 0 \tag{13}$$

Concerning the *resistance component* of the power signal $\{P_t^r\}$, i.e., due to ordinary motion resistances expressed as $r_t = \sum_{j=0}^{2}\beta_j v_t^j$, the element-wise product $\{r_t\} \odot \{v_t\}$ is, see Eq. (4):

$$P_t^r = r_t v_t = \sum_{j=0}^{2}\beta_j\left(v_0 + \sum_{i=1}^{t} a_i\Delta t\right)^{j+1} \tag{14}$$

The resulting total energy consumption due to resistances is:

$$EC_T^r = T\Delta t v_0\sum_{j=0}^{2}\beta_j v_0^j + \sum_{j=0}^{2}\beta_j\sum_{t=1}^{T}\left(\sum_{i=1}^{t} a_i\Delta t^2\right)^{j+1} \tag{15}$$

Recalling the notation $a$, and noting that Eq. (15) is a 3rd order polynomial of $a$, *the expected value and the variance of the resistance component of the total consumption, $EC_T^r$, are a function of the acceleration variance $\sigma_a^2$* (see $\Phi$ in the following equation), similar to $EC_T^{in}$. In particular, the expected value is:

$$\mathrm{E}\left[EC_T^r\right] = T\Delta t v_0\sum_{j=0}^{2}\beta_j v_0^j + \Phi\left(\sigma_a^4\right) \tag{16}$$

If speed dynamics are neglected in Eq. (16), i.e., $\sigma_a = 0$, the expected value of $EC_T^r$ becomes:

$$\mathrm{E}\left[EC_T^r\right]_{\sigma_a=0} = T\Delta t v_0\sum_{j=0}^{2}\beta_j v_0^j \tag{17}$$

Therefore:

$$\mathrm{E}[EC_T]_{\sigma_a=0} = \mathrm{E}\left[EC_T^{in}\right]_{\sigma_a=0} + \mathrm{E}\left[EC_T^r\right]_{\sigma_a=0} = T\Delta t v_0\sum_{j=0}^{2}\beta_j v_0^j \tag{18}$$

In conclusion, the percentage error, i.e., the consumption underestimation of assuming $\sigma_a = 0$ (see Eqs. (12a), (16) and (18)):

$$\frac{\mathrm{E}[EC_T]_{\sigma_a=0} - \mathrm{E}[EC_T]}{\mathrm{E}[EC_T]} = -\frac{k\sigma_a^2\Delta t^2 + \Phi\left(\sigma_a^4\right)}{T\Delta t v_0\sum_{j=0}^{2}\beta_j v_0^j + k\sigma_a^2\Delta t^2 + \Phi\left(\sigma_a^4\right)} \tag{19}$$

which is not negligiblec. For example, for a 5.5 ton electric minivan, with a payload of 2.5 ton, an average speed $v_0 = 10$ m/s, a duration T = 100 s, an acceleration variance $\sigma_a^2 = 2\ m^2/s^4$, road load coefficients $\beta_0 = 0.0787$, $\beta_1 = 5.6 \bullet 10^{-4}$, $\beta_2 = 0.5441$, the EV energy consumption underestimation ranges from 79% for a constant regenerative braking efficiency equal to 0.3, to 35%, for an efficiency equal to 0.9.

## 4. Impact of modelling uncertainties on the variability of simulated vehicle energy consumption

### 4.1. Methodology

The theoretical investigation in Section 3 is useful to identify the existence of a modelling bias i.e., the energy consumption underestimation and spot its causes. Because of simplifying modelling assumptions (see e.g., constant regenerative braking, or no road slope resistances), this analytical approach is not appropriate to accurately quantify such bias. More detailed models have been

[3] It can be proved that, considering autocorrelation in the acceleration signal the expected value of the total consumption in Eq. (12a) does not change (Papoulis, 1984). With regards to the variance – see Eq. (12b) – we note that the acceleration autocorrelation increases the variance of accelerations and then consumption. In real driving, autocorrelation is positive for short lags (e.g. 1–2 s) and loses a physical meaning for longer lags, indeed (i.e., for longer gaps, the oscillation of autocorrelation around zero is not statistically significant).

therefore applied through numerical simulation.

The models were run in a Monte Carlo framework, where both model parameters and inputs such as speed and slope profiles were sampled to account for different sources of uncertainty in vehicle energy consumption. According to good practice in modelling, rather than mapping a single set of inputs into a single inference, in this approach a model is used to map uncertain inputs (i.e., distributions) into an interval of inferences (Saltelli et al., 2020). In fact, investigating a nonlinear model in the neighbourhood of nominal conditions, or in specific scenarios, leave the analyst entirely blind on the actual model behaviour in most of the input space i.e., when a model faces with real-world conditions (Saltelli and Annoni, 2010). The production of model-based inference in the form of empirically generated distribution of outputs values is commonly known as *uncertainty analysis*. The inverse process of linking the uncertainty in the inference to the uncertainty in the inputs is known as *sensitivity analysis*. Results from the latter are relevant to identify what inputs or parameters are most influential on the model inference, i.e., energy consumption error in this case (see Punzo and Montanino, 2020, for an introduction to uncertainty modelling in traffic modelling).

The whole investigation, which tailors uncertainty and sensitivity analyses to EV energy consumption modelling, follows the methodological flow in Fig. 1.

In this methodology, non-parametric inputs and model parameters are sampled, in a quasi-random Monte Carlo setting (see more details in Section 4.2). Speed and slope input profiles are generated from the sampled non-parametric inputs by means of algorithms specifically devised to emulate their real-world variability (see Section 4.3).[4] For each generated set of speed and slope profiles and sampled parameters, the EV energy consumption is calculated by means of both the microscopic and macroscopic models in Eqs. (1) and (2). Such uncertainty propagation results in the distributions of (simulated) energy consumption (SEC) for both the models.

To study the accuracy of such models, the discrepancy between the simulated SEC values and a *laboratory* SEC provided by a reference model is calculated for both the models (referred as model error, $\varepsilon$, in the figure). As reference model, a calibrated version of the model in Genikomsakis and Mitrentsis (2017) is adopted, whose error on a wide set of international driving cycles ranges from 3 to 7%, according to the same study. Real world consumptions could not be used as reference values indeed, as they cannot cover the needed full-factorial variability of the inputs (see the design of experiment in Section 4.2). However, to account for a possible bias introduced by the reference model, the variability of model errors against real-world measurements has been also investigated (see Section 6).

A variance-based global sensitivity analysis is then applied to disentangle the impact on model error of the two main sources of input uncertainty (i.e., speed/slope profiles, and parameters). As a major result of this analysis the impact of the *average inputs* assumption on the accuracy of predicted energy consumption is evaluated (see Hp in Fig. 1). This analysis significantly extends the study by Fiori et al. (2021a), by considering uncertain vehicle speed and road slope profiles.

Based on a Sobol's variance decomposition (Sobol, 2001), the first-order sensitivity index, $S_i$, and the total sensitivity index, $ST_i$, of each input factor $i$, are computed. These indices describe the contribution to the unconditional error variance of a factor, both by the factor alone (first-order effect), and by the factor in interaction with all the others (total effect). For a review of Sobol's indices definition, please refer to Saltelli et al. (2010).

### 4.2. Design of experiment

Global uncertainty and sensitivity analysis are methods which explore the whole space of the input factors, based on the consideration that a handful of data points judiciously sampled from that space is far more effective, in the sense of being informative and robust, than estimating a model and its derivatives at a single data point in the centre of the space (Saltelli et al., 2008). Therefore, Monte Carlo samples of input factors were obtained through Sobol's quasi random number sequences (Sobol, 1967) which guarantee a faster convergence of numerical integral calculations (see the sensitivity indices) than other sequences such as Halton's or pseudo-random numbers (Saltelli et al., 2010).

Uncertain non-parametric inputs and model parameters were assumed to be independent uniform random variables.[5] As to the non-parametric inputs, $\boldsymbol{u}$, the following factors were considered: the mean speed, $\mu_v$, the standard deviation of the acceleration, $\sigma_a$ (a zero mean $\mu_a$ was assumed, as in Section 3), the mean road slope, $\mu_\theta$, and the standard deviation of road slope, $\sigma_\theta$, the vehicle load, $w$, and the link length, $L$. The speed and slope profiles were generated through the algorithms in Section 4.3, by sampling values of $\mu_v$, $\sigma_a$, $\mu_\theta$, $\sigma_\theta$ and $L$ (in this application, Gaussian distribution models were adopted for both vehicle acceleration and road slope[6]).

The microscopic power-based model by Fiori and Marzano (2018), and its macroscopic model counterpart, were adopted to simulate energy consumption. The uncertain model parameters, $\boldsymbol{\beta}$, included in the analysis were the rolling resistance parameter, $f$, the frontal section coefficient, $A_f$, the drag coefficient, $C_d$, the overall powertrain efficiency, $\eta$ (including motor, driveline and battery efficiencies), and the coefficient of the regenerative braking system model, $\alpha$.

Table 1 lists all the uncertain factors, reporting the selected lower and upper bounds of each uniform distribution. The bounds were

[4] Other external factors may affect vehicle energy consumption, such as the ambient temperature. However, they are not considered here being this study focused on the impact of vehicle dynamics. With regards to ambient temperature, for instance, the reader can refer to Hao et al. (2020).

[5] When no a-priori information is available on the input distribution, a conservative assumption is to adopt independent uniform distributions (Saltelli et al., 2008).

[6] Although the numerical results could change if a distribution model other than Gaussian were adopted in the calculations, we anticipate here that the magnitude of the estimated impacts of acceleration and slope on consumption suggests that the main analysis outcomes would remain unchanged (see Section 4.4).

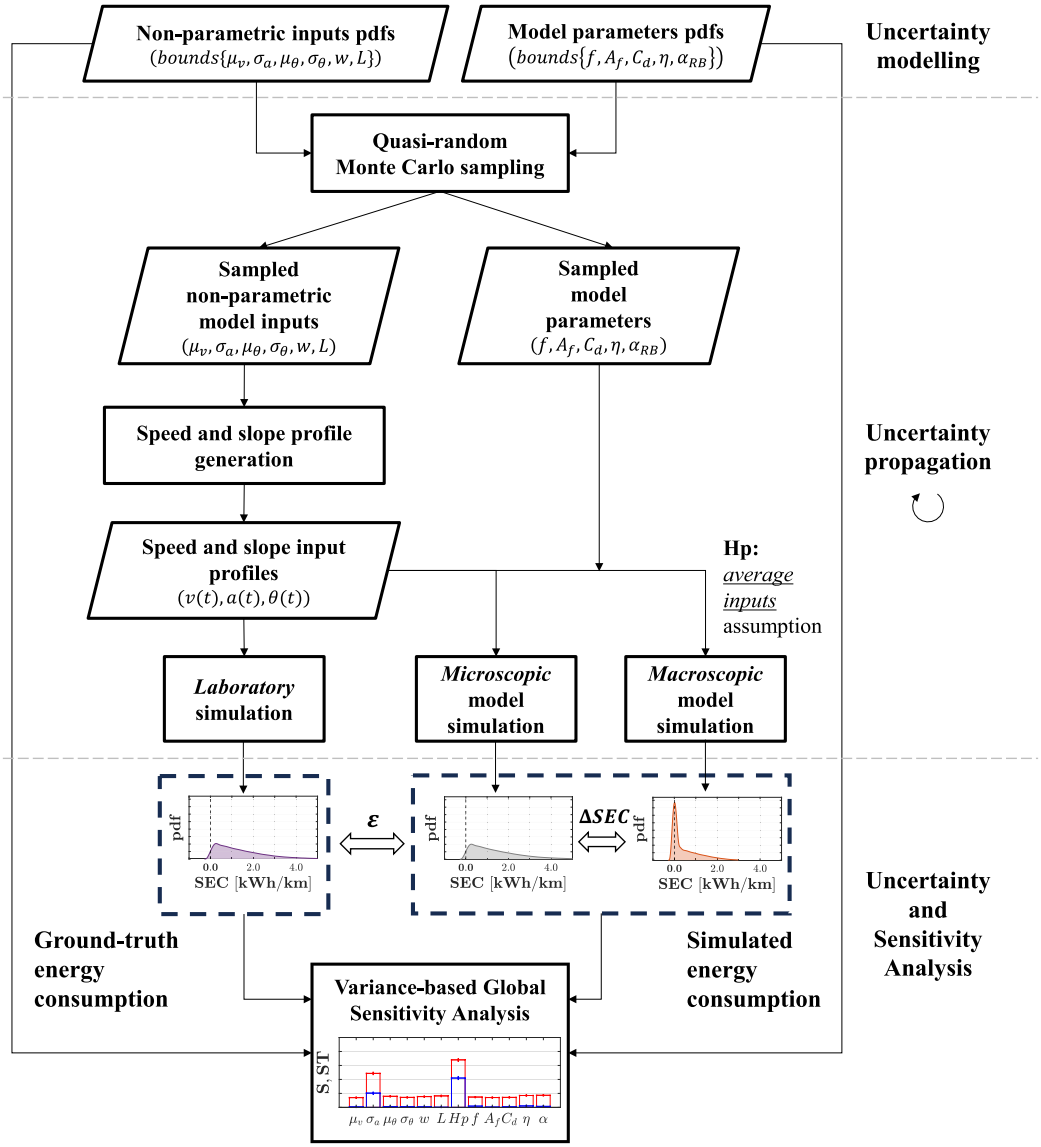


**Fig. 1.** Methodological framework.

**Table 1**
List of uncertain factors and corresponding lower (LB) and upper (UB) bounds of uniform distributions.

| Non-parametric inputs | LB | UB |
|---|---|---|
| Mean speed, $\mu_v$ [km/h] | 5.0 | 130.0 |
| Acceleration standard deviation, $\sigma_a$ [m/s$^2$] | 0.0 | 3.50 |
| Mean road slope,$\mu_\theta$ | −0.05 | 0.05 |
| Road slope standard deviation,$\sigma_\theta$ | 0.00 | 0.05 |
| Vehicle load, $w$ [kg] | 0 | 2500 |
| Link length, $L$ [m] | 100 | 2000 |
| **Model parameters** | **LB** | **UB** |
| Rolling resistance parameter,$f$ | 0.005 | 0.020 |
| Frontal section area, $A_f$ [m$^2$] | 0.70 | 0.90 |
| Drag coefficient,$C_d$ | 0.10 | 0.50 |
| Powertrain efficiency,$\eta$ | 0.70 | 0.90 |
| Regenerative braking coefficient,$\alpha$ | 0.00 | 5.00 |

chosen to represent the variability of operations that may occur in the real-world as much as possible (with respect to e.g., vehicle characteristics, road conditions and traffic). Please note that, the vehicle kerb mass was fixed to 5.5 ton (which equals the mass of the electric minivan tested in Fiori and Marzano, 2018). In addition, the auxiliary systems were not included in the analysis, since related consumption is independent from driving dynamics.

Uncertain factors were sampled according to the designs in Jansen (1999) and Saltelli et al. (2010), which are conceived for the efficient computation of Sobol's first-order and total-order indices, respectively.

To investigate the impact of the *average inputs* assumption of the macroscopic model on the variability of the model prediction error, a further uncertain factor was included in the experimental design. That is a Boolean variable whose values correspond to the model structure – microscopic or macroscopic – applied in SEC computation. In other words, at each Monte Carlo run, both the inputs and the model were sampled.

Accordingly, a total number of 1,835,008 model simulations were run to explore the impact of the uncertain factors on consumption error variability and compute the sensitivity indices ($1{,}835{,}008 = 2^{17} \cdot (\mathrm{K}+2)$, where $\mathrm{K} = 12$ is the total number of uncertain factors).

### 4.3. Vehicle speed and road slope profile generation

#### 4.3.1. Speed profile generation

The algorithm objective is to generate a speed profile which has a mean, $\mu_v$, and a first derivative with a zero-mean (i.e., $\mu_a = 0$) and a given standard deviation, $\sigma_a$. Applying the algorithm in a Monte Carlo framework produces a population of speed profiles that incorporates the sought variability of $\mu_v$ and $\sigma_a$ (see discussion in Section 3).

A sketch of the proposed speed profile generation algorithm is presented in Fig. 2.

The conceptual steps of the algorithm depicted therein, are as follows: first, a speed signal, $\widehat{V}(t)$, is calculated by integrating a given acceleration signal, $a(t)$, with $\mu_a = 0$ and a standard deviation, $\sigma_a$. The resulting speed signal (see the *grey curve*) might assume unphysical, i.e., negative values, and might have a mean speed $\overline{\widehat{V}}$ different from $\mu_v$. Thus, the problem consists in making this speed profile nonnegative, with a mean $\mu_v$, without altering the zero-mean and the standard deviation of its first derivative, $\sigma_a$. To this aim, the speed signal $\widehat{V}(t)$ is shifted by $\mu_v - \overline{\widehat{V}}$ (see the *black curve*), producing a speed profile with the desired mean speed $\mu_v$, but (potentially) still having some negative speed values (the *red–black curve* portion). Thus, the negative values are set to zero, and the remaining positive speed profile (the *gold-black curve* portion) is shifted down by an amount equal to the integral of the cancelled negative speed values (see the final *green curve*, that is shifted to make the *light blue area equal to the light red area*). Eventually, additional treatments to the shifted speed signal (that cannot be represented in the figure) are applied to restore the desired standard deviation of its first derivative, $\sigma_a$.

A detailed description of the algorithm steps is provided below, including some theorems necessary to prove the truthfulness of the procedure.

As a first step, given a mean speed, $\mu_v$, an acceleration standard deviation, $\sigma_a$, and a time duration, $T$, an acceleration signal $a(t)$, $t \in [0, T]$, is sampled e.g., from a Gaussian process with zero mean and standard deviation $\sigma_a$.[7] To preserve physical consistency of the acceleration process, a resorting is applied to sampled values to avoid jerk absolute values higher than 10 m/s$^3$, and more than one jerk sign inversion in a one-second time window (see Punzo et al., 2011). These constraints introduce an autocorrelation in the acceleration signal de facto.

Let $\widehat{V}(t) = \int_0^t a(t')dt'$ be the acceleration integral function (see the *grey curve* in the figure), whose integral mean $\overline{\widehat{V}} = \frac{1}{T}\int_0^T \widehat{V}(t)dt$. A translation of $\widehat{V}(t)$ by the quantity $\mu_v - \overline{\widehat{V}}$ returns a speed profile $\widehat{v}(t)$ with integral mean equal to $\mu_v$ (see the *black curve* in the figure). That is:

$$\widehat{v}(t) = \widehat{V}(t) + \mu_v - \overline{\widehat{V}} \tag{20}$$

From Eq. (20), the integral mean of $\widehat{v}(t)$ $= \frac{1}{T}\int_0^T \widehat{v}(t)dt = \frac{1}{T}\int_0^T \widehat{V}(t)dt + \mu_v - \overline{\widehat{V}} = \mu_v$.

The speed profile $\widehat{v}(t)$ in Eq. (20), however, may exhibit negative values (see the *red–black curve* portion). Therefore, the speed profile generation problem consists in finding a nonnegative function $v(t) \geq 0, \forall t \in [0, T]$, that satisfies the following requirements:

a) the integral mean $\overline{v} = \frac{1}{T}\int_0^T v(t)dt$ is equal to $\mu_v$,
b) the integral mean of its first derivative $\overline{\dot{v}} = \frac{1}{T}\int_0^T \dot{v}(t)dt$ is equal to 0,
c) the standard deviation of its first derivative $\sigma_{\dot{v}} = \sqrt{\frac{1}{T}\int_0^T [\dot{v}(t) - \overline{\dot{v}}]^2 dt}$ is equal to $\sigma_a$.

By decomposing the function $\widehat{v}(t)$ in the sum of its positive and negative parts, i.e., $\widehat{v}(t) = \widehat{v}^+(t) + \widehat{v}^-(t)$, where $\widehat{v}^+(t) = max\{\widehat{v}(t), 0\}$ and $\widehat{v}^-(t) = min\{\widehat{v}(t), 0\}$, and posing $\widehat{v}^-(t) = 0$ to ensure nonnegativity, a candidate function $v(t)$ can be formulated as $v(t) =$

[7] A normal distribution is assumed here for simplicity, without loss of generality. Notwithstanding, the assumption is verified in reconstructed NGSIM I80-1 data (Montanino and Punzo, 2015), for small acceleration sample sizes i.e., up to 100 acceleration values.

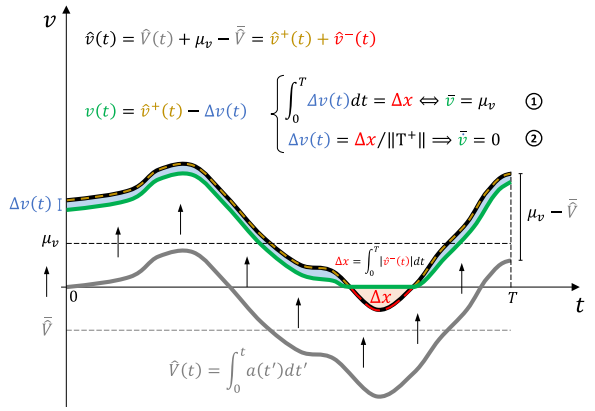


**Fig. 2.** Sketch of the proposed speed profile generation algorithm, based on the conditions derived in Theorem 1 and 2. The integral of accelerations, $\hat{\boldsymbol{V}}(\boldsymbol{t})$, with integral mean $\bar{\hat{\boldsymbol{V}}}$, is drawn in grey, while the translated speed profile, $\hat{\boldsymbol{v}}(\boldsymbol{t})$, with integral mean $\boldsymbol{\mu_v}$, in black. The positive and negative parts of $\hat{\boldsymbol{v}}(\boldsymbol{t})$, i.e., $\hat{\boldsymbol{v}}^+(\boldsymbol{t})$ and $\hat{\boldsymbol{v}}^-(\boldsymbol{t})$, are drawn in gold and red, respectively. The final speed profile, $\boldsymbol{v}(\boldsymbol{t})$, in green, results from the subtraction of $\Delta\boldsymbol{v}(\boldsymbol{t})$, in blue, to $\hat{\boldsymbol{v}}(\boldsymbol{t})$, in order to ensure the nonnegativity of $\boldsymbol{v}(\boldsymbol{t})$, preserve the integral mean $\boldsymbol{\mu_v}$ (Theorem 1) and a zero integral mean of its first derivative (Theorem 2). (For interpretation of the references to colour in this figure legend, the reader is referred to the web version of this article.)

$\hat{v}^+(t) - \Delta v(t)$, where $\Delta v(t)$ can be designed in order to meet requirements (a-c) listed above. In particular, it can be shown that the following is a sufficient condition to satisfy requirements (a) and (b).

$$v(t) = \hat{v}^+(t) - \Delta v(t) \tag{21a}$$

$$\Delta v(t) = \begin{cases} \dfrac{\int_{t\in T^-} |\hat{v}(t)|dt}{\|T^+\|} & \forall t \in T^+ \\ 0 \end{cases} \tag{21b}$$

where $T^- = \{t \in T | v(t) < 0\}$ ($T^+$ is defined analogously).

The proof is based on the following theorems.

**Theorem 1.** *Given two differentiable and Riemann integrable real functions* $\hat{f} : X \subset \mathbb{R}^+ \to \mathbb{R}$ *and* $f : X \subset \mathbb{R}^+ \to \mathbb{R}$, *with* $\hat{f}(x) = \hat{f}^+(x) + \hat{f}^-(x)$, *being* $\hat{f}^\pm(x) = \begin{cases} \hat{f}(x), \forall x \in X^\pm \subset \mathbb{R}^+ \\ 0 \end{cases}$ *with* $X^+ = \{x \in X | \hat{f}(x) > 0\}$, $X^- = \{x \in X | \hat{f}(x) < 0\}$, *and* $f(x) = \hat{f}^+(x) - g(x), \forall x \in \mathbb{R}^+$ *with* $g : X \subset \mathbb{R}^+ \to \mathbb{R}^+$, *then*:

$\int_{x\in X} g(x)dx = \int_{x\in X^-} |\hat{f}(x)|dx$ *is a necessary and sufficient condition for* $\int_{x\in X} f(x)dx = \int_{x\in X} \hat{f}(x)dx$ *(see proof in Appendix A.1).*

**Theorem 2.** *Given the functions* $\hat{f}(x)$ *and* $f(x)$ *defined in Theorem* 1, *then*:

$$g(x) = \begin{cases} \dfrac{1}{\|X^+\|} \displaystyle\int_{x\in X^-} |\hat{f}(x)|dx, \forall x \in X^+ \subset \mathbb{R}^+ \\ 0 \end{cases}$$ *is a sufficient condition for* $\int_{x\in X} f(x)dx = \int_{x\in X} \hat{f}(x)dx$ *and* $\int_{x\in X} \dot{f}(x)dx = \int_{x\in X} \dot{\hat{f}}(x)dx$

*(see proof in Appendix A.2).*

However, the speed profile $v(t)$ in Eq. (21) (see the *green curve* in the figure) may have a first derivative $\dot{v}(t)$ with standard deviation, $\sigma_{\dot{v}}$, not equal to $\sigma_a$ (requirement (c) is not met). In fact, 'cutting out' the portion of accelerations that yields $\hat{v}(t) < 0$ (see the *red–black curve* portion) may alter the standard deviation of the accelerations (though preserving its zero mean integral, as a consequence of the Newton–Leibniz theorem).

Therefore, in order to find a suitable function $\Delta v^*(t)$ that guarantees requirements (a-c), a nonlinear optimization problem can be formulated as:

$$\gamma^* = \underset{\gamma}{\operatorname{argmin}} \min_{t\in[0,T]} |\Delta v^*(t,\gamma) - \Delta v(t)| \tag{22}$$

$$s.t. \int_0^T \Delta v^*(t,\gamma)dt = \int_0^T |\hat{v}^-(t)|dt \tag{23}$$

$$\int_0^T \dot{\hat{v}}^+(t)dt - \int_0^T \Delta\dot{v}^*(t,\gamma)dt = 0 \tag{24}$$

$$\sqrt{\frac{1}{\|\mathrm{T}\|}\int_0^T [\dot{\widehat{v}}^{+}(t) - \Delta\dot{v}^{*}(t,\boldsymbol{\gamma})]^2 dt} = \sigma_a \tag{25}$$

where $\Delta v(t)$ is defined in Eq. (21b) and $\Delta v^*(t,\boldsymbol{\gamma}) = \sum_{i=0}^{5}\gamma_i t^i$ is a 5-degree polynomial function. The optimization problem in Eq. (22) consists of finding the polynomial coefficients $\boldsymbol{\gamma}^*$ that minimize the minimum distance between $\Delta v^*$ and $\Delta v$. Constraints in Eqs. (23)–(25) guarantee that the requirements (a-c) are met.

An alternative way to restore requirement (c) in $v(t)$ from Eq. (21), under specific circumstances, consists in a standardization and scaling of $\dot{v}(t)$, as follows:

$$\dot{v}^*(t) = (\dot{v}(t) - \overline{\dot{v}})\frac{\sigma_a}{\sigma_{\dot{v}}} \tag{26}$$

Eq. (26) ensures that $\overline{\dot{v}^*} = 0$ and $\sigma_{\dot{v}^*} = \sigma_a$ (clearly, if $\frac{\sigma_a}{\sigma_{\dot{v}}} = 1$, the transformation in Eq. (26) is not needed). Noting that $\overline{\dot{v}} = \mu_a = 0$ (see Theorem 2), the integral function $V^*(t) = \int_0^t \dot{v}^*(t')dt'$ is equal to:

$$V^*(t) = V(t)\cdot\frac{\sigma_a}{\sigma_{\dot{v}}} \tag{27}$$

where $V(t) = \int_0^t \dot{v}(t')dt'$ (it is worth noting that, $V(t)$ differs from $\widehat{V}(t)$ in Eq. (20), since $V(t)$ results from 'cutting out' the portion of $a(t), \forall t \in \mathrm{T}^-$ in order to ensure that requirements (a-b) are met, see also Fig. 2).

From Eq. (27), it yields:

$$\overline{V^*} = \overline{V}\cdot\frac{\sigma_a}{\sigma_{\dot{v}}} \tag{28}$$

By subtracting Eq. (28) to Eq. (27) and applying the min operator, it results $min\{V^*(t) - \overline{V^*}\} = min\{V(t) - \overline{V}\}\cdot\frac{\sigma_a}{\sigma_{\dot{v}}}$. Therefore, the speed profile $v^*(t)$ resulting from the translation of $V^*(t)$ as in Eq. (20), has an integral mean equal to $\mu_v$ and a minimum value equal to:

$$min\{v^*(t) - \mu_v\} = min\{v(t) - \mu_v\}\cdot\frac{\sigma_a}{\sigma_{\dot{v}}} \tag{29}$$

Theorem 3 proves that $\frac{\sigma_a}{\sigma_{\dot{v}}} < 1$ is a necessary and sufficient condition to obtain a nonnegative speed profile $v^*(t)$. Therefore, under such condition, the transformation in Eq. (26) returns a speed profile that meets requirements (a-c).

**Theorem 3.**. *Given two continuous functions* $f : \mathrm{X}\subset\mathbb{R}^+\to\mathbb{R}^+$ *and* $f^* : \mathrm{X}\subset\mathbb{R}^+\to\mathbb{R}^+$ *such that* $min\{f(x)\} = 0$ *and* $min\{f^*(x) - \mu\} = min\{f(x) - \mu\}\cdot\xi, \forall\mu,\xi \in \mathbb{R}^+\setminus\{0\}$*, then:*

$\xi < 1$ is a necessary and sufficient condition for $min\{f^*(x)\} > min\{f(x)\}$ (see proof in Appendix A.3).

The condition $\frac{\sigma_a}{\sigma_{\dot{v}}} < 1$ is satisfied if the portion of $a(t)$ that is set to zero in Eq. (21), i.e., $\forall t \in \mathrm{T}^-$, contains values which are close to the mean (please note that the Newton–Leibniz theorem ensures that the mean in $\mathrm{T}^-$ is zero, i.e., $\int_{t\in\mathrm{T}^-} a(t)dt = 0$). In fact, if the portion of accelerations which are set to zero has little variability from the mean, it contributes little to the variance of the accelerations.

Conversely, if $\frac{\sigma_a}{\sigma_{\dot{v}}} > 1$, the resulting $v^*(t)$ needs to be transformed again according to Eqs. (21) and (26). This procedure is iterated until $\frac{\sigma_a}{\sigma_{\dot{v}}} < 1$, though it cannot be proved that it converges, i.e., that a nonnegative speed profile is obtained. In fact, convergence has been observed in 83% out of the $2^{17}$ speed profiles generated in the experiment described in Section 4.2. Of course, in case convergence is not reached in a predefined maximum number of iterations (*maxIter*), the generated speed profile is rejected, and the algorithm restarts from the beginning. The complete procedure is reported in Algorithm 1 ($\in$ being a small numerical threshold). A sample of generated speed profiles is shown in Fig. 4.

**Algorithm 1 – Speed profile generation algorithm**

1: $T \leftarrow round((L/\mu_v)/dt)$
2: $\boldsymbol{a} \leftarrow inv\_pdf(random(T), 0, \sigma_a)$
3: $\boldsymbol{a} \leftarrow resort(\boldsymbol{a})$
4: $\dot{\boldsymbol{v}} \leftarrow \boldsymbol{a}, \sigma_{\dot{v}} \leftarrow \infty, iter \leftarrow 0$
5: **while** $abs(\sigma_{\dot{v}} - \sigma_a) > \in$ **do**
6: $\quad\widehat{\boldsymbol{V}} \leftarrow [0, cumsum(\dot{\boldsymbol{v}})\cdot dt]$
7: $\quad\widehat{\boldsymbol{v}} \leftarrow max\{0, \widehat{\boldsymbol{V}} + \mu_v - mean(\widehat{\boldsymbol{V}})\}$ (see Eq. (20))
8: $\quad\Delta x \leftarrow sum(|\widehat{\boldsymbol{v}}^-|\cdot dt)$
9: $\quad$**if** $\Delta x \geq 0$
10: $\quad\quad\boldsymbol{v} \leftarrow max\{0, \widehat{\boldsymbol{v}}^+ - \Delta x/(\|\mathrm{T}^-\|\cdot dt)\}$ (see Eq. (21))
11: $\quad\quad\sigma_{\dot{v}} \leftarrow std(\dot{\boldsymbol{v}})$
12 $\quad\quad\dot{\boldsymbol{v}} \leftarrow \dot{\boldsymbol{v}}\cdot(\sigma_a/\sigma_{\dot{v}})$ (see Eq. (26))
13: $\quad\quad iter \leftarrow iter + 1$
14 $\quad\quad$**if** $iter > maxIter$ **go to** line 2
15: $\quad$**else**

(*continued on next page*)

(*continued*)

**Algorithm 1 – Speed profile generation algorithm**

| | |
|---|---|
| 16 | $\boldsymbol{v} \leftarrow \widehat{\boldsymbol{v}}$ |
| 17: | $\sigma_{\dot{v}} \leftarrow std(\dot{\boldsymbol{v}})$ |
| 18: | $\boldsymbol{v}^* \leftarrow \boldsymbol{v}$ |

#### 4.3.2. *Road slope profile generation*

The objective is to smooth a road slope profile $\theta(x(t)), t \in [0, T]$ resulting from a realization of a random process e.g., Gaussian, with mean $\mu_\theta$ and standard deviation $\sigma_\theta$ (being $x(t)$ the longitudinal vehicle position), without altering the slope values, thus preserving the mean and the standard deviation.

In the literature, there exist many filters that smooth the signal while preserving the integral mean $\mu_\theta$, either naturally (see, for instance, Savitzky-Golay filter or the boxcar filter with normalization), or after offsetting of the smoothed signal. By means of standardization and scaling (as in Eq. (26)), also the desired standard deviation $\sigma_\theta$ can be restored. However, available filters permanently alter the data values. Moreover, they can hardly ensure that the variation of the gradient between consecutive points falls within a desired range of variation. Therefore, to solve this problem, a *stochastic reshuffling* algorithm is proposed to avoid altering the data values (thus preserving $\mu_\theta$ and $\sigma_\theta$), and controlling the desired range of variation between consecutive points.

The core idea of Algorithm 2 is illustrated in Fig. 3.

Basically, it consists of swapping an *incompatible* slope value at position $x$ (see point $k+1$ in the figure), i.e., a value whose variation from the previous one exceeds the desired threshold (see $\epsilon_\theta$), with a *compatible* value randomly sampled from those downstream of $x$. The resulting road slope profile, therefore, contains the same slope values of the original profile (i.e., with mean $\mu_\theta$ and standard deviation $\sigma_\theta$), but reshuffled so that the slope variation between every pair of consecutive points falls within a desired range.

Given a point $k \in \mathrm{K}$ of the sampled slope profile (see the *green point*), if the absolute slope variation between points $k+1$ and $k$ is greater than a threshold $\epsilon_\theta/2$, i.e., $|\theta_{k+1} - \theta_k| > \epsilon_\theta/2$, the point $k+1$ (see the *red filled circle*) is swapped with a point that follows $k+1$ (see the *dashed green filled circle* $c_3$) that is randomly selected among points $\mathrm{C}(\theta_k) = \{c_j : |\theta_j - \theta_k| \le \epsilon_\theta/2\} \subseteq \mathrm{K}(k)$, with $\mathrm{K}(k)$ being the non-empty subset of K composed by points that follow $k$: $\mathrm{C}(\theta_j) = \{c_z : |\theta_z - \theta_j| \le \epsilon_\theta/2\} \subseteq \mathrm{K}(k) \backslash \{j\} \neq \varnothing$. The last condition ensures that the selection of a point is rejected if there are no compatible points following it (see e.g., $c_N$).

Before executing the algorithm described above, a check is made to see if, for any point, there is at least one other compatible point that follows it, after sorting the sampled slope data by increasing values (see the function check($\boldsymbol{\theta}$) at line 3 of Algorithm 2).

A sample of generated road slope profiles is shown in Fig. 4.

**Algorithm 2 – Road slope profile generation algorithm**

| | |
|---|---|
| 1: | $T \leftarrow round(L/(\mu_v/dt))$ |
| 2: | $\boldsymbol{\theta} \leftarrow inv\_pdf(random(T), \mu_\theta, \sigma_\theta)$ |
| 3: | **do** : $\boldsymbol{\theta} \leftarrow inv\_pdf(random(T), \mu_\theta, \sigma_\theta)$ **while** check($\boldsymbol{\theta}$) = true |
| 4: | $\boldsymbol{\theta}^* \leftarrow \boldsymbol{\theta}$ |
| 5: | **for** $k \in \mathrm{K}$ |
| 6: | $\mathrm{C} = \mathrm{C}(\theta_k^*) \leftarrow \{j \in \mathrm{K}(k) : |\theta_j - \theta_k^*| \le \epsilon_\theta/2 \cap \mathrm{C}(\theta_j) \subseteq \mathrm{K}(k) \backslash \{j\} \neq \varnothing\}$ |
| 7: | $s \leftarrow random(\mathrm{C})$ |
| 8: | $\theta_{k+1}^* \leftarrow \theta_s$ |
| 9: | $\theta_s^* \leftarrow \theta_{k+1}$ |

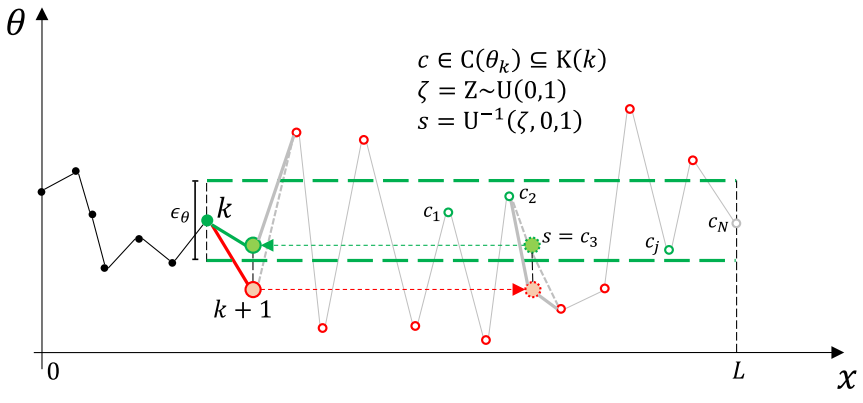


**Fig. 3.** Sketch of the *stochastic reshuffling* algorithm for road slope profile smoothing.

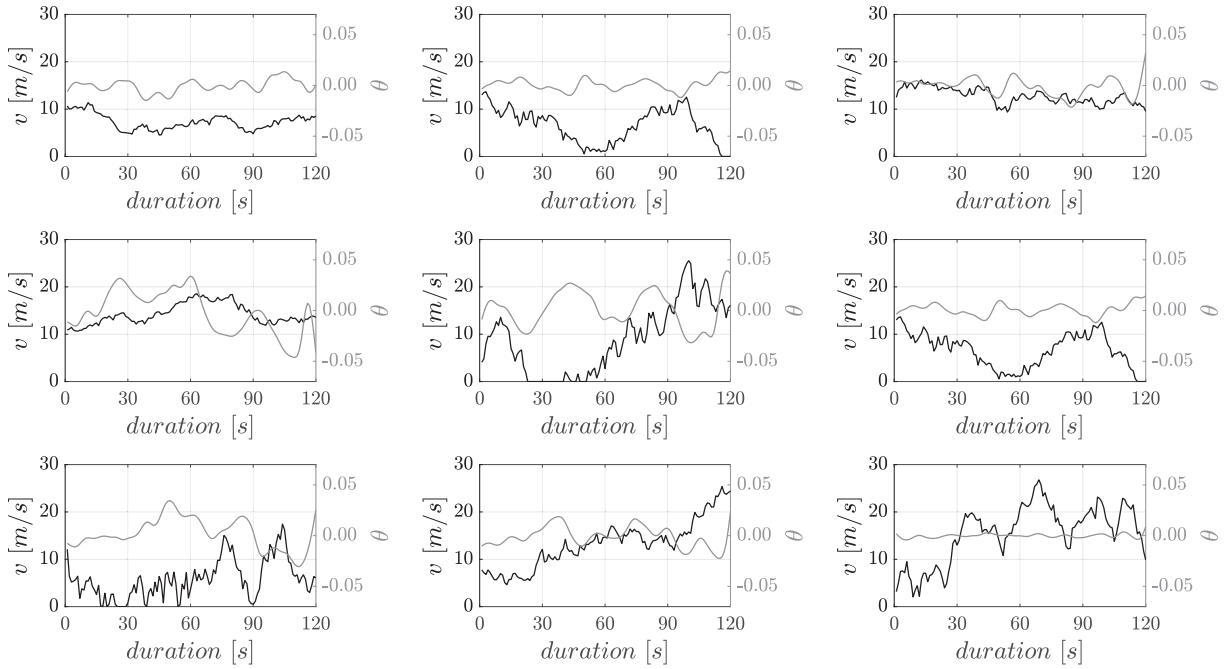


**Fig. 4.** Sample of synthetic vehicle speed and road slope profiles. For the sake of visual representation, profiles with the same duration, but different space travelled, are shown.

### *4.4. Uncertainty and sensitivity analysis results*

The scatter plots in Fig. 5 show the simulation errors of the macroscopic and microscopic models. For each simulation $i$, the error $\varepsilon_i$ has been computed as follows:

$$\varepsilon_i = \frac{EC_{model}(\boldsymbol{u_i}, \boldsymbol{\beta_i}) - EC_{synthetic}(\boldsymbol{u_i})}{L_i} \tag{30}$$

where $EC_{model}$ is the simulated total energy consumption on the link of length $L_i$ by the microscopic/macroscopic model fed with the model parameters $\boldsymbol{\beta_i}$ and the speed/slope profiles generated by the algorithms in Section 4.3 according to the non-parametric inputs $\boldsymbol{u_i}$; and $EC_{synthetic}$ is the laboratory energy consumption computed by means of the reference model (Genikomsakis and Mitrentsis, 2017) fed with the same input profiles. A positive error means that the model overestimate consumption, a negative value implying an underestimation.

In the scatter plots, the simulation errors are plotted against each analysis factor. In the top row, there are the scatter plots against the non-parametric inputs; in the bottom row, the scatter plots against the model parameters but the last factor, which refers to the modelling assumption *Hp* (i.e., macro or micro) in the form of a box plot. We make the most of having a Boolean factor, i.e., the modelling assumption, to distinguish errors in the plots per model, and get a deeper insight into the analysis results. In fact, dark grey and orange points depict microscopic and macroscopic model errors, respectively, so that the impact of any factor on consumption errors can be separately observed for the two models.

A first comment on results in Fig. 5, is that *the macroscopic model significantly underestimates consumption in most of the simulations*, see the bottom rightmost plot (the median error value is -0.85 kWh/km – see the red horizontal line – while the 85th and 90th percentiles are -0.16 and -0.07 kWh/km, respectively). Conversely, the microscopic model is unbiased. It has the same probability of overestimating or underestimating consumption, and it exhibits a much lower error variance than the macroscopic model (0.30 vs. 0.91 kWh/km). These results overall confirm theoretical findings in Section 3.

Concerning the other scatter plots, *light grey* and *yellow* points depict the average SEC error of the microscopic and macroscopic model, respectively, as it varies over a factor range. *Blue* points depict the average SEC error independently on the chosen model (i.e., they are calculated on the totality of simulation results). Given a factor, the higher the variance of light grey and yellow points over that factor, the higher the influence of that factor on the variation of the average SEC error of microscopic and macroscopic model, respectively; whereas, the blue points variance is a proxy of the factor influence independently on the chosen model. In general, the variance of average points represents the first-order effect or main effect of a given factor on the output variance (Saltelli et al., 2010), that is its standalone impact without considering the interactions with other factors.

The $\sigma_a$ scatter plot is the most interesting. Clearly, $\sigma_a$ is one of the only two factors which have a significant first-order effect on the error variance, the other being the modelling assumption *Hp* (see the variance of the *blue* points). A deeper look at the plot, suggests that the first-order impact of $\sigma_a$ on the error variance materializes only when the macroscopic model is used, see the non-zero variance

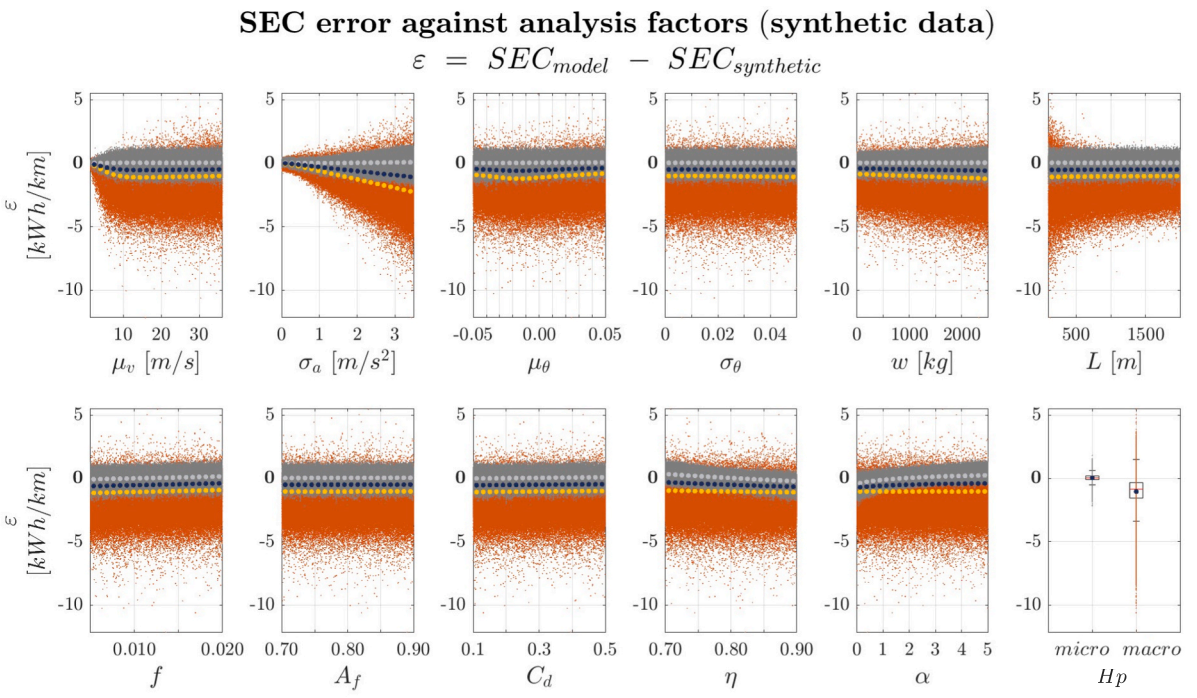


**Fig. 5.** Scatter plots of the microscopic and macroscopic models *SEC errors* relative to the laboratory ground-truth. In the top row *SEC errors* are projected over non-parametric inputs; in the bottom row against model parameters, except for the last plot on the right, which refers to the modelling assumption *Hp*. In all plots, dark grey and orange points refer to the microscopic and macroscopic model, respectively. Light grey and yellow points depict the average errors of the microscopic and macroscopic model, respectively, over the full range of variation of a factor. Blue points depict the average error, whatever the modelling assumption *Hp* value. (For interpretation of the references to colour in this figure legend, the reader is referred to the web version of this article.)

of *yellow* points (macro) vs. the zero variance of the *light grey* points (micro). This consideration suggests that the modelling bias of the macroscopic model quantified in the bottom rightmost plot, is an increasing function of the acceleration standard deviation, $\sigma_a$. The higher the value of $\sigma_a$, the higher the (negative) bias of results, which was expected as $\sigma_a = 0$ is a major assumption of the macroscopic model. In other words, *neglecting the variability of the input speed profile significantly affects model accuracy* (and impedes the identification of worst-case consumption scenarios suggested in Pelletier et al., 2019).

For the microscopic model, despite the variance of the error averages is zero i.e., the *light grey* points lie horizontally over $\sigma_a$ (which means that $\sigma_a$ has no impact at the first-order on the model error variance), the conical pattern of the *dark grey* points suggests that $\sigma_a$ still retains some influence on the error variance, due to the interaction with other factors. In fact, the higher $\sigma_a$, the higher the microscopic model error variance.

In general, interaction effects are captured by the total sensitivity index $ST_i$ that, for any factor $i$, quantifies the total contribution of that factor to the output variance (in this case, to the SEC error variance), i.e., the sum of the main effect and the interaction effects of any order with the other factors.[8]

First-order and total sensitivity indices are reported in Fig. 6 for all factors (that are the non-parametric inputs, the modelling assumption *Hp*, and the model parameters). Sensitivity indices confirm that all factors but $\sigma_a$ and the modelling assumption *Hp*, have an impact on the error variance only in interaction with other factors. Concerning $\sigma_a$, a deeper analysis reveals that more than the 90% of its interaction effects is due to its second-order interaction with the modelling assumption *Hp*, that is $S_{\sigma_a,Hp}/(ST_{\sigma_a} - S_{\sigma_a}) = 0.24/0.26$ (in the figure, the sum of all interaction effects is the difference $ST_{\sigma_a} - S_{\sigma_a}$ between the red and blue bar). Furthermore, the second-order interaction between $\sigma_a$ and the modelling assumption *Hp*, $S_{\sigma_a,Hp}$, also accounts for almost all the interaction effects of *Hp* (see the *Hp* bars in the figure). As the interactions effects of $\sigma_a$ and *Hp* with all other factors are almost negligible, the interaction effects of such remaining factors are almost completely due to their reciprocal interactions of any order (i.e., all but those including $\sigma_a$ and *Hp*).

In conclusion, $\sigma_a$ and the modelling assumption *Hp* are the only factors that have a first-order impact on the SEC error variance, that is they would have an impact also if their interaction effects with all other factors were neglected. When considering also the interaction effects (see the red bars) they are by far the factors that mostly influence the SEC error variance and the bias.

[8] Given $k$ factors, the total sensitivity index of a factor $i$, $ST_i = S_i + \sum_{j\neq i} S_{ij} + \sum_{j\neq i}\sum_{p\neq i,j} S_{ijp} + \cdots + \sum_{j\neq i}\sum_{p\neq i,j}\cdots\sum_{k\neq i,j,p,\ldots} S_{ijp\cdots k}$, where the first term, $S_i$, is the first-order sensitivity index, the second term is the summation of the second-order sensitivity indices, $S_{ij}$, and so on.

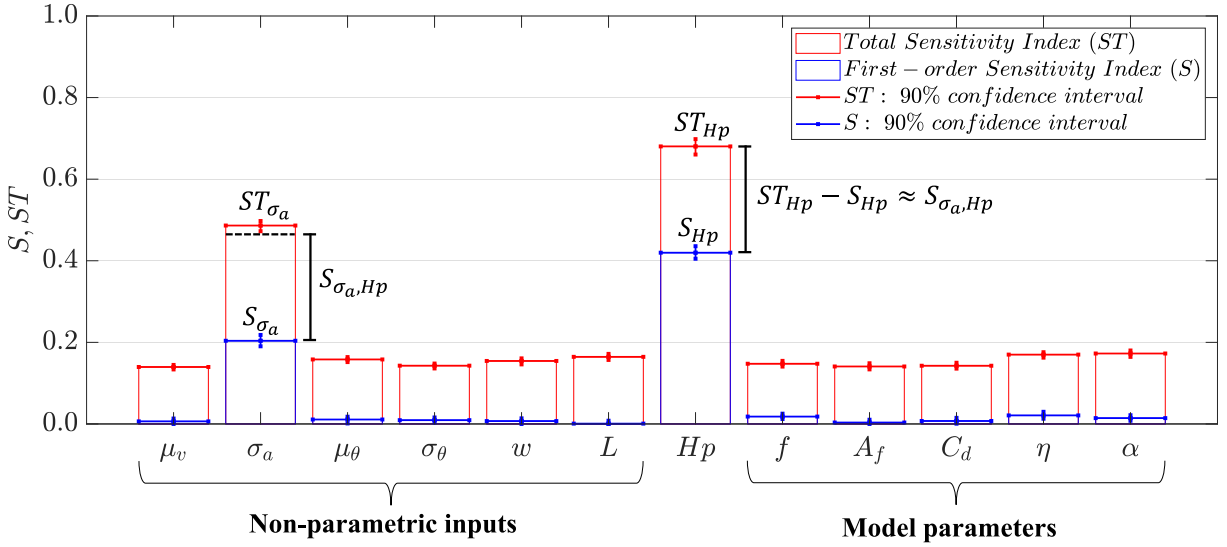


**Fig. 6.** First-order and total sensitivity indices of the analysis factors.

Therefore, as macroscopic models neglect traffic dynamics by imposing a constant speed profile, i.e., $\sigma_a = 0$, and this causes a significant bias on consumption, and much higher errors than considering $\sigma_a \neq 0$, the robustness of consumption predictions by a macroscopic model is seriously questioned. The goal of the next section is to remedy this modelling deficiency.

## 5. Traffic-flow-dependent macroscopic model of electric vehicle energy consumption

In this section, macroscopic energy consumption models of electric vehicles are augmented to correct the prediction bias, i.e., the underestimation of consumption. As such bias is primarily caused by neglecting traffic dynamics (see $\sigma_a$), a model component is added to explain the 'average' variability of consumption due to prevailing traffic conditions.

Since microscopic models show a consistent behaviour in mimicking vehicle energy consumption (see the unbiased and low variance consumption error distribution in the box plot in Fig. 5), the aim of the proposed extension is to make the predictions of a macroscopic model as accurate as those provided by a microscopic model (the consumption error returned by the microscopic model in Eq. (1) is the lower bound for the macroscopic model in Eq. (2), indeed). Therefore, for each model simulation $i$, a measure of discrepancy between the two models, once fed with the same inputs $\boldsymbol{u_i}$ and $\boldsymbol{\beta_i}$, is defined as follows:

$$\Delta SEC(\boldsymbol{u_i}, \boldsymbol{\beta_i}) = SEC_{macro}(\boldsymbol{u_i}, \boldsymbol{\beta_i}) - SEC_{micro}(\boldsymbol{u_i}, \boldsymbol{\beta_i}) \tag{31}$$

where $SEC_{macro}$ is the value returned by the macroscopic model and $SEC_{micro}$ the one returned by its microscopic counterpart. A negative value of $\Delta SEC$ means that the macroscopic model underestimates microscopic model consumption.

Fig. 7 presents the scatter plots of $\Delta SEC$ against the non-parametric input factors $\boldsymbol{u_i}$, and against $\sigma_v$, which is not an input factor.[9]

In accordance with the theoretical findings in Section 3, the scatter plots clearly highlight that the standard deviation of acceleration, $\sigma_a$, explains the systematic consumption underestimation of the macroscopic model relative to the microscopic one. As expected, being the standard deviation of speed, $\sigma_v$, a function of $\sigma_a$ (see Eq. (5b)), also $\sigma_v$ significantly affects $\Delta SEC$. In turn, the road slope profile, as described by $\mu_\theta$ and $\sigma_\theta$, does not influence the $\Delta SEC$ (see bottom plots in Fig. 7) – though it obviously affects the $SEC$.

To make the macroscopic model unbiased (relative to the microscopic one), two alternative formulations are provided. These models are obtained by augmenting the macroscopic model with a model component equal to the bias, expressed either as a function of $\sigma_a$ or $\sigma_v$ (see the green and blue curves in Fig. 7, respectively):

$$EC_{macro}^{aug(\sigma_a)} = EC_{macro} + \beta_{\sigma_a}\sigma_a \tag{32}$$

$$EC_{macro}^{aug(\sigma_v)} = EC_{macro} + \frac{\beta_{\sigma_v,1}}{1 + \beta_{\sigma_v,2}/\sigma_v} \tag{33}$$

where $\beta_{\sigma_a}$, $\beta_{\sigma_v,1}$ and $\beta_{\sigma_v,2}$ are model constants.

By bootstrapping generated speed profiles and macroscopic model parameters, the 90% confidence intervals of $\beta_{\sigma_a}, \beta_{\sigma_v,1}$ and $\beta_{\sigma_v,2}$ resulted: $\beta_{\sigma_a} = 0.74 \pm 0.04, \beta_{\sigma_v,1} = 3.3 \pm 0.8, \beta_{\sigma_v,2} = 6.6 \pm 2.1$.

[9] $\sigma_v$ is not an input of the model, as speed profiles are generated from $\sigma_a$ and $\mu_v$. Therefore, it has been computed from the generated speed profiles.

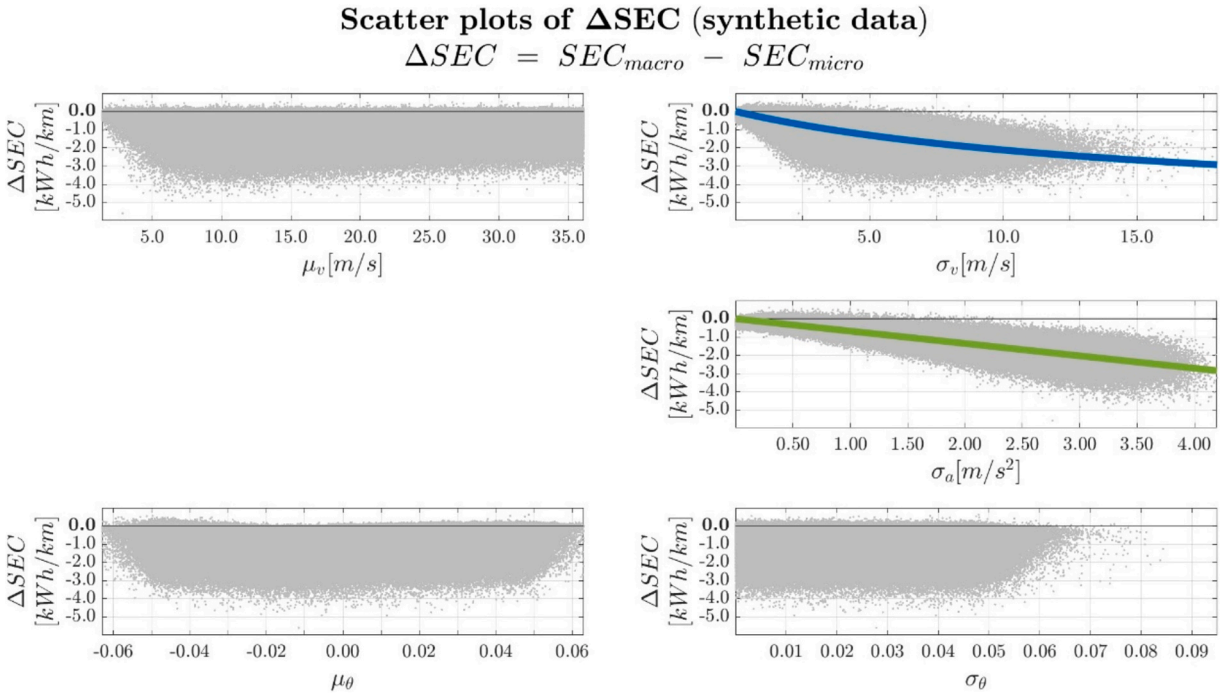


**Fig. 7.** Scatter plots of the difference between the SEC values returned by the macroscopic and microscopic models, relative to non-parametric model inputs.

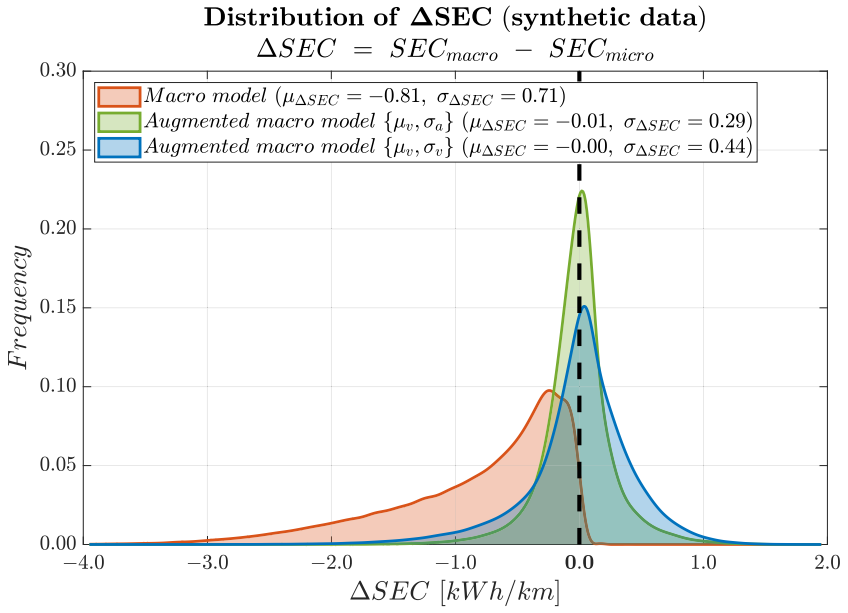


**Fig. 8.** Δ***SEC*** distributions of the macroscopic model (orange), the $\sigma_a$-based (green) and the $\sigma_v$-based (blue) augmented models. (For interpretation of the references to colour in this figure legend, the reader is referred to the web version of this article.)

To compare performances of both augmented and base models, simulations were run according to the design of experiment in Section 4. Fig. 8 depicts the distributions of Δ*SEC* returned by the base macroscopic model (orange curve), and by the two augmented models, i.e., the $\sigma_a$-based (green curve) and $\sigma_v$-based (blue curve) one. As expected, *the negative bias of the macroscopic model is corrected by both the proposed models* (the mean value of Δ*SEC* moves from -0.81 kWh/km for the base model to zero for the new ones). As to the variance, the $\sigma_a$-based variant yields a higher reduction than the $\sigma_v$-based relative to the base model (from 0.71 to either 0.29 or 0.44 kWh/km for the two variants, respectively).

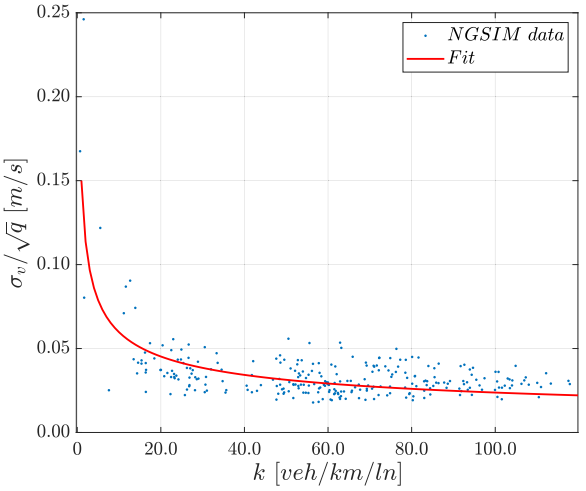


**Fig. 9.** Empirical relationship among the standard deviation of individual vehicle speeds ($\boldsymbol{\sigma_v}$), the traffic density ($\boldsymbol{k}$) and flow ($\boldsymbol{q}$), in the reconstructed NGSIM I-80 vehicle trajectory data. The quantities are calculated at a time–space resolution of 60 s × 500 m.

Among the proposed augmented models, the $\sigma_a$-based formulation is the best. However, currently, this formulation is hardly applicable in a real-world case, as vehicle accelerations are not usually available (though they are likely to become readily available in a near future). On the contrary, there exists a relationship among the standard deviation of speeds, $\sigma_v$, and measurable traffic characteristics, namely, the traffic density, $k$, and the flow, $q$, on a link. Fig. 9 shows the relationship among these quantities obtained by processing the reconstructed NGSIM I80-1 vehicle trajectory dataset. This dataset depicts the trajectories of all vehicles in a time–space domain of 15 min × 500 m at a resolution of 10 Hz. Therefore, it provides a consistent ground-truth between microscopic and macroscopic traffic resolutions.

The best interpolating function of experimental points is (see the red curve in Fig. 9):

$$\sigma_v = \gamma_1 k^{-\gamma_2} q^{0.5} \tag{34}$$

where $\gamma_1$ and $\gamma_2$ are two positive constants ($\gamma_1 = 0.3$, $\gamma_2 = 0.4$). Eq. (34) extends findings in Bai et al. (2021), which were obtained for vehicle speed values of vehicles at detectors, to time-series of instantaneous vehicle speeds. In fact, Eq. (34) describes the decrease in the variance of vehicles speed caused by the increase in mutual vehicle interactions in more congested traffic. Therefore, the shape of the curve in Eq. (34) is not expected to vary significantly from one location to another, being the result of physical rather behavioural conditioning (for the same reason it is instead expected to vary with environmental factors such as the rainfall intensity, as this influences the traffic speed level and vehicle interactions; see Bai et al., 2021).

By Eqs. (33)–(34):

$$EC^{aug(k,q)}_{macro(\mu_v)} = EC_{macro(\mu_v)} + \frac{\beta_{\sigma_v,1}}{1 + \beta_{\sigma_v,2}/(\gamma_1 k^{-\gamma_2} q^{0.5})} \tag{35}$$

Eq. (35) formulates an augmented model in which the consumption aliquot captured by the added component depends on the link density and flow.[10] In other words, Eq. (35) depicts the energy consumption of an electric vehicle in response to prevailing traffic conditions.

It is worth noting that, the notation $EC_{macro(\mu_v)}$ in Eq. (35) makes the dependence of the consumption on the average vehicle speed on a link, $\mu_v$, explicit. If available from traffic measurements, the space mean speed $\overline{v_s}$ can replace $\mu_v$ in Eq. (35), yielding a macroscopic energy consumption model that depends only on macroscopic traffic characteristics[11]:

$$EC_{macro(\overline{v_s})^{aug(k,q)}} = EC_{macro(\overline{v_s})} + \frac{\beta_{\sigma_v,1}}{1+\beta_{\sigma_v,2}/(\gamma_1 k^{-\gamma_2} q^{0.5})} \tag{36}$$

To compare the discrepancy from microscopic model consumptions ($\Delta SEC$) of the base macroscopic model (either fed with $\mu_v$ or $\overline{v_s}$) and the proposed traffic-flow-dependent augmented models (Eqs. (35–36)), quasi-random Monte Carlo model simulations were performed by sampling vehicle trajectories from the NGSIM dataset, and model parameters from the distributions in Table 1. Fig. 10 shows the distributions of $\Delta SEC$ returned by the two variants of the base macroscopic model (light and dark orange curves), and the two variants of the augmented model (light and dark blue curves).

Results show that the augmented models sensibly reduce the average discrepancy from the microscopic model (-0.57 vs. -1.34 for

[10] For practical purposes, a proxy of the density of a link can be used instead, that is the detector occupancy.

[11] For practical purposes, a proxy of the space mean speed can be calculated from observed cross-sectional speed data, as their harmonic mean.

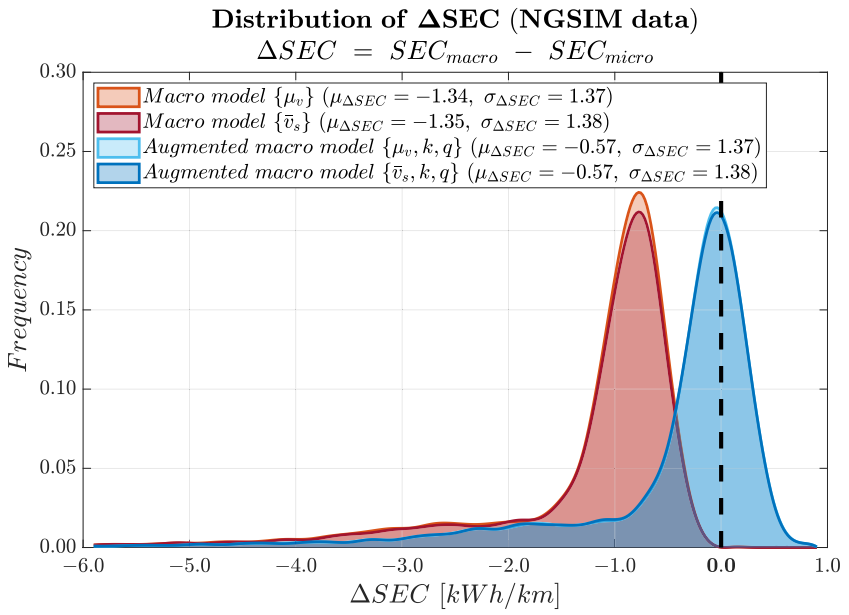


**Fig. 10.** Δ***SEC*** distributions of the macroscopic model and proposed traffic-flow-dependent augmented models, on reconstructed NGSIM I-80 dataset. Colours refer to model variants obtained by using, as input, the average speed of each individual vehicle ($\boldsymbol{\mu_v}$), or the traffic space mean speed ($\overline{\boldsymbol{v_s}}$). Light and dark orange curves refer to the variants of the base macroscopic model, while light and dark blue curves to the variants of the proposed augmented model. (For interpretation of the references to colour in this figure legend, the reader is referred to the web version of this article.)

the augmented and base models, respectively). Moreover, no substantial difference on the vehicle consumption distribution was found if individual vehicle consumptions are computed basing on individual vehicle mean speed $\mu_v$, or on the common value of the space mean speed $\overline{v_s}$ (either in the base model or in the augmented one).

## 6. Model validation

Results discussed so far are based on a laboratory ground-truth. In this section, the variability of the prediction error of the base macroscopic model and its $\sigma_v$-based augmented version is studied using real-world vehicle energy consumption data. Data are taken from Fiori and Marzano (2018) and consists of paired 1 Hz trajectory and powertrain data collected during daily pickup and delivery operations of a fleet of electric freight vehicles in the city centre of Rome (Italy). Further details on the data collection can be found in Fiori and Marzano (2018).

As to the model parameters, the calibrated values reported in Fiori and Marzano (2018) were adopted. For the $\sigma_v$-based augmented model, the values of $\beta_{\sigma_v,1}$ and $\beta_{\sigma_v,2}$ calibrated on the synthetic data were applied (see Section 5).

To verify the impact of the link segmentation level on model accuracy, four levels of segmentation were considered, i.e. 100 m, 200 m, 500 m and 1000 m. Therefore, for the sake of the analysis, vehicle trajectories with a length greater than or equal to 1 km were selected (73 out of 115) and divided into segments of equal length. For each vehicle trajectory segment *i*, the vehicle energy consumption was simulated by *i)* the microscopic model in Fiori and Marzano (2018), *ii)* the macroscopic model obtained by feeding the model in Fiori and Marzano (2018) with the average vehicle speed and road slope of the segment, and *iii)* the $\sigma_v$-based augmented macroscopic model. The model error on SEC, $\varepsilon_i$, was then computed as follows:

$$\varepsilon_i = \frac{EC_{model}(\boldsymbol{x_i}, \boldsymbol{\beta_i}) - EC_{observed}(\boldsymbol{x_i})}{L_i} \tag{37}$$

where $EC_{model}$ is the simulated total energy consumption on segment $i$ of length $L_i$ by the (microscopic/macroscopic/augmented) model fed with measured inputs $\boldsymbol{x_i}$ (speed/slope profiles, vehicle load, auxiliary system power) and model parameters $\boldsymbol{\beta_i}$; $EC_{observed}$ is the observed vehicle energy consumption. A positive error means that the model overestimates observed consumption, a negative value implying an underestimation.

Fig. 11 shows the distributions of the SEC errors for the three models at different segmentation levels. As expected, the microscopic model is the most accurate in predicting vehicle energy consumption (the error mean, in absolute term, and the standard deviation are the lowest among the tested models, for all segmentation levels).

Regarding the macroscopic models, the mean error of the $\sigma_v$-based augmented model is consistently lower (in absolute term) than that of the base model, for all segmentation levels, and becomes progressively closer to that of the microscopic model as the segmentation level increases (for 1 km-length segments, the mean errors are equal). Conversely, the base macroscopic model substantially

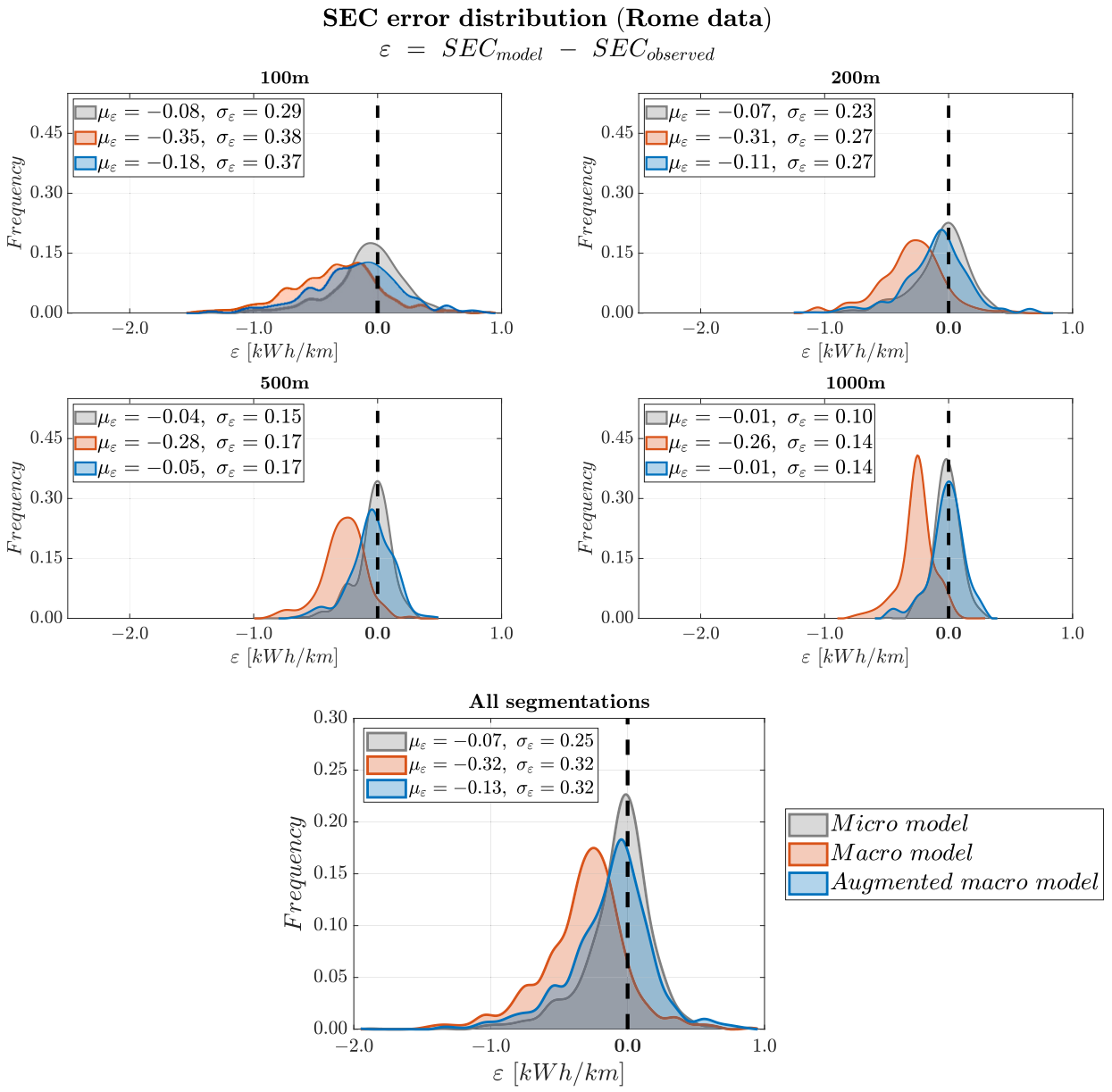


**Fig. 11.** SEC error distributions of the microscopic model (grey), the base macroscopic model (orange) and the proposed $\sigma_v$-based augmented macroscopic model (blue), relative to the experimental data. (For interpretation of the references to colour in this figure legend, the reader is referred to the web version of this article.)

underestimates consumptions at all segmentation levels (the mean value ranges between -0.35 and -0.26 kWh/km). As to the error variance, no difference was found between the base and the augmented model.

## 7. Conclusion

Macroscopic energy consumption models are essential for several electric mobility systems, especially to solve related problems, see e.g., electric vehicle routing optimization.

In this study, it is analytically demonstrated that the assumption of constant link speed, which is customarily adopted in macroscopic models, yields a significant underestimation of vehicle energy consumption. This modelling bias is shown to be the result of neglecting the variance of vehicle acceleration that is neglecting traffic conditions. Such a theoretical finding has been corroborated by a comprehensive simulation experiment, which overcomes the restrictive assumptions of the analytical investigation and allows macroscopic models to be compared with their microscopic counterparts thoroughly, i.e., in an uncertain input space emulating the

real-world variability of inputs such as vehicle speed and road slope profiles, and plausible model parameter ranges. To this aim, algorithms to generate realistic input profiles have been additionally devised.

The uncertainty and sensitivity analyses following the numerical simulations showed that, among inputs, the road slope variance has a negligible effect on the mentioned bias of a macroscopic energy consumption model relative to its microscopic counterpart. Therefore, to correct this bias a function of either the acceleration or speed variance (the latter being a convenient proxy of the former) is used to augment the base macroscopic model. Speed variance, in particular, is found to be empirically related to easily measurable macroscopic traffic characteristics such as link density and flow. Eventually, this result led us to reformulate the augmented macroscopic energy consumption model as a function of macroscopic traffic characteristics. Validation against laboratory and experimental data showed that the proposed model is consistently more accurate than the base macroscopic one.

The devised traffic-flow-dependent macroscopic energy consumption model is particularly suitable for integration into static and dynamic macroscopic traffic flow models, which is a crucial feature for the design and operation of several electric mobility services and infrastructures.

We remark that the simulation-based approach adopted in this study is not optional. Nonlinearity and non-additivity of a model leave the analyst entirely blind on its actual behaviour when the model is evaluated only in the neighbourhood of nominal inputs or parameters, and in specific scenarios. Inputs and parameters interaction effects cannot be disregarded indeed (sometimes they are even higher than first-order effects) and dictate that a thorough exploration of the entire plausible input space is applied to evaluate a model. Uncertainty and sensitivity analyses are good modelling practice that serve to this purpose.

Future research includes the calibration of the relationship between vehicle speed variance and macroscopic traffic characteristics in different contexts and traffic conditions, and the framework extension to ICE vehicles.

## CRediT authorship contribution statement

**Marcello Montanino:** Writing – review & editing, Writing – original draft, Visualization, Validation, Supervision, Software, Project administration, Methodology, Investigation, Funding acquisition, Formal analysis, Conceptualization. **Ilaria Natale:** Writing – review & editing, Writing – original draft, Visualization, Software, Methodology, Investigation, Formal analysis, Data curation, Conceptualization. **Chiara Fiori:** Writing – review & editing, Writing – original draft, Validation, Software, Methodology, Investigation, Formal analysis, Data curation, Conceptualization. **Vincenzo Punzo:** Writing – review & editing, Writing – original draft, Visualization, Validation, Supervision, Project administration, Methodology, Investigation, Funding acquisition, Formal analysis, Conceptualization.

## Declaration of competing interest

The authors declare that they have no known competing financial interests or personal relationships that could have appeared to influence the work reported in this paper.

## Acknowledgments

Research in this paper has been partially funded by the EU's Horizon Europe project "ACUMEN" (Grant Agreement ID 101103808).

## Appendix A

### *A.1 Proof of Theorem 1*

By applying the integral operator to $f(x) = \widehat{f}^{+}(x) - g(x)$, it yields:

$$\int_{x\in X} f(x)dx = \int_{x\in X} \widehat{f}^{+}(x)dx - \int_{x\in X} g(x)dx \tag{A1}$$

Since $\int_{x\in X} g(x)dx = \int_{x\in X^{-}} |\widehat{f}(x)|dx$ and noting that, by definition, $\int_{x\in X^{-}} |\widehat{f}(x)|dx = -\int_{x\in X} \widehat{f}^{-}(x)dx$, Eq. (A1) becomes:

$$\int_{x\in X} f(x)dx = \int_{x\in X} \widehat{f}^{+}(x)dx + \int_{x\in X} \widehat{f}^{-}(x)dx = \int_{x\in X} \widehat{f}(x)dx \tag{A2}$$

which proves sufficiency.

By replacing the definition of $f(x)$ and $\widehat{f}(x)$ in $\int_{x\in X} f(x)dx = \int_{x\in X} \widehat{f}(x)dx$, it yields:

$$\int_{x\in X} \widehat{f}^{+}(x)dx + \int_{x\in X} \widehat{f}^{-}(x)dx = \int_{x\in X} \widehat{f}^{+}(x)dx - \int_{x\in X} g(x)dx \tag{A3}$$

Eq. (A3) is verified only if $\int_{x\in X} g(x)dx = -\int_{x\in X} \widehat{f}^{-}(x)dx = \int_{x\in X^{-}} |\widehat{f}(x)|dx$, which proves necessity.

*A.2 Proof of Theorem 2*

Since $g(x)$ is a constant in $X^+$ and equals 0 in $X^-$, its integral over X is:

$$\int_{x\in X} g(x)dx = g(x)\|X^+\| \tag{A4}$$

Provided the definition of $g(x)$, it yields:

$$\int_{x\in X} g(x)dx = \int_{x\in X^-} |\widehat{f}(x)|dx \tag{A5}$$

Therefore, Eq. (A5) and Theorem 1 prove sufficiency for the first condition.

In addition, provided the definition of $f(x)$, and that $g(x)$ is a constant in $X^+$ and equals 0 in $X^-$:

$$\dot{f}(x) = \dot{\widehat{f}}^{+}(x) \tag{A6}$$

By applying the integral operator to Eq. (A6):

$$\int_{x\in X} \dot{f}(x)dx = \int_{x\in X} \dot{\widehat{f}}^{+}(x)dx \tag{A7}$$

Provided the definition of $\widehat{f}(x)$, it yields:

$$\int_{x\in X} \dot{\widehat{f}}(x)dx = \int_{x\in X} \dot{\widehat{f}}^{+}(x)dx + \int_{x\in X} \dot{\widehat{f}}^{-}(x)dx \tag{A8}$$

Since, by definition, $\widehat{f}^{-}(x) = 0, \forall x \in X^+ \cup \{\inf\{S_i\}, \sup\{S_i\}\}, \forall S_i : \bigcup_{i=1}^{N} S_i = X^-$, from the Newton–Leibniz theorem it follows that: $\int_{x\in X} \dot{\widehat{f}}^{-}(x)dx = 0$. Therefore, Eq. (A6) becomes:

$$\int_{x\in X} \dot{\widehat{f}}(x)dx = \int_{x\in X} \dot{\widehat{f}}^{+}(x)dx \tag{A9}$$

which proves sufficiency for the second condition.

*A.3 Proof of Theorem 3*

Given that $\frac{min\{f^*(x)-\mu\}}{min\{f(x)-\mu\}} = \xi$, if $\xi < 1$, it yields:

$$\frac{min\{f^*(x)-\mu\}}{min\{f(x)-\mu\}} < 1 \tag{A10}$$

Provided that $min\{f(x)\} = 0$, it yields that $min\{f(x)-\mu\} < 0, \forall \mu \in \mathbb{R}^+\backslash\{0\}$. Therefore, inequality in Eq. (A10) becomes:

$$min\{f^*(x)-\mu\} > min\{f(x)-\mu\} \rightarrow min\{f^*(x)\} > min\{f(x)\} \tag{A11}$$

which proves sufficiency.

Conversely:

$$min\{f^*(x)\} > min\{f(x)\} \rightarrow min\{f^*(x)\} - \mu > min\{f(x)\} - \mu, \forall \mu \in \mathbb{R}^+\backslash\{0\} \tag{A12}$$

Eq. (A12) implies:

$$min\{f^*(x)-\mu\} > min\{f(x)-\mu\} \tag{A13}$$

Since $min\{f(x)-\mu\} < 0$, it yields:

$$\frac{min\{f^*(x)-\mu\}}{min\{f(x)-\mu\}} = \xi < 1 \tag{A14}$$

which proves necessity.

## References


Adler, J.D., Mirchandani, P.B., 2016. The vehicle scheduling problem for fleets with alternative-fuel vehicles. Transp. Sci. 51 (2), 441–456.

Avishan, F., Yanıkoğlu, İ., Alwesabi, Y., 2023. Electric bus fleet scheduling under travel time and energy consumption uncertainty. Transp. Res. Part C Emerging Technol. 156, 104357.

Bai, L., Wong, S.C., Xu, P., Chow, A.H.F., Lam, W.H.K., 2021. Calibration of stochastic link-based fundamental diagram with explicit consideration of speed heterogeneity. Transp. Res. B Methodol. 150, 524–539.

Basso, R., Kulcsár, B., Egardt, B., Lindroth, P., Sanchez-Diaz, I., 2019. Energy consumption estimation integrated into the electric vehicle routing problem. Transp. Res. Part D: Transp. Environ. 69, 141–167.

Bektas, T., Laporte, G., 2011. The pollution-routing problem. Transp. Res. B Methodol. 45 (8), 1232–1250.

Bi, Z., Keoleian, G.A., Ersal, T., 2018. Wireless charger deployment for an electric bus network: a multi-objective life cycle optimization. Appl. Energy 225, 1090–1101.

Bongiovanni, C., Kaspi, M., Geroliminis, N., 2019. The electric autonomous dial-a-ride problem. Transp. Res. B Methodol. 122, 436–456.

Brooker, A., Gonder, J., Wang, L., Wood, E., Lopp, S., Ramroth, L., 2015. FASTSim: A Model To Estimate Vehicle Efficiency, Cost, and Performance. SAE Technical Paper, 2015-01-0973.

Demir, E., Bektas, T., Laporte, G., 2014. A review of recent research on green road freight transportation. Eur. J. Oper. Res. 237 (3), 775–793.

Desaulniers, G., Errico, F., Irnich, S., Schneider, M., 2016. Exact algorithms for electric vehicle-routing problems with time windows. Oper. Res. 64 (6), 1388–1405.

Dong, J., Liu, C., Lin, Z., 2014. Charging infrastructure planning for promoting battery electric vehicles: an activity-based approach using multiday travel data. Transp. Res. Part C Emerging Technol. 38, 44–55.

Erdogan, S., Miller-Hooks, E., 2012. A green vehicle routing problem. Transp. Res. Part E: Logist. Transp. Rev. 48 (1), 100–114.

Esmaeilnejad, S., Kattan, L., Wirasinghe, S.C., 2023. Optimal charging station locations and durations for a transit route with battery-electric buses: a two-stage stochastic programming approach with consideration of weather conditions. Transp. Res. Part C Emerging Technol. 156, 104327.

Felipe, Á., Ortuño, M.T., Righini, G., Tirado, G., 2014. A heuristic approach for the green vehicle routing problem with multiple technologies and partial recharges. Transp. Res. Part E: Logist. Transp. Rev. 71, 111–128.

Fiori, C., Ahn, K., Rakha, H.A., 2016. Power-based electric vehicle energy consumption model: model development and validation. Appl. Energy 168, 257–268.

Fiori, C., Marzano, M., 2018. Modelling energy consumption of electric freight vehicles in urban pickup/delivery operations: analysis and estimation on a real-world dataset. Transp. Res. Part D: Transp. Environ. 65, 658–673.

Fiori, C., Marzano, V., Punzo, V., Montanino, M., 2021a. Energy consumption modeling in presence of uncertainty. IEEE Trans. Intell. Transp. Syst. 22 (10).

Fiori, C., Montanino, M., Nielsen, S., Seredynski, M., Viti, F., 2021b. Microscopic energy consumption modelling of electric buses: model development, calibration, and validation. Transp. Res. Part D: Transp. Environ. 98, 102978.

Fontana, M.W., 2013. Optimal Routes for Electric Vehicles Facing Uncertainty, Congestion, and Energy Constraints. Ph.D. dissertation thesis. Massachusetts Institute of Technology. https://dspace.mit.edu/handle/1721.1/84715 (last accessed on August 29th, 2024).

Franceschetti, A., Honhon, D., Woensel, T.V., Bektas, T., Laporte, G., 2013. The time-dependent pollution-routing problem. Transp. Res. B Methodol. 56, 265–293.

Gallet, M., Massiera, T., Hamacher, T., 2018. Estimation of the energy demand of electric buses based on real-world data for large-scale public transport networks. Appl. Energy 203, 344–356.

Genikomsakis, K.N., Mitrentsis, G., 2017. A computationally efficient simulation model for estimating energy consumption of electric vehicles in the context of route planning applications. Transp. Res. Part D: Transp. Environ. 50, 98–118.

Goeke, D., Schneider, M., 2015. Routing a mixed fleet of electric and conventional vehicles. Eur. J. Oper. Res. 245 (1), 81–99.

Hao, X., Wang, H., Lin, Z., Ouyang, M., 2020. Seasonal effects on electric vehicle energy consumption and driving range: a case study on personal, taxi, and ridesharing vehicles. J. Clean. Prod. 249, 119403.

He, F., Yin, Y., Zhou, J., 2015. Deploying public charging stations for electric vehicles on urban road networks. Transp. Res. Part C Emerging Technol. 60, 227–240.

Hiermann, G., Hartl, R.F., Puchinger, J., Vidal, T., 2019. Routing a mix of conventional plug-in hybrid, and electric vehicles. Eur. J. Oper. Res. 272 (1), 235–248.

Hjelkrem, O.A., Lervåg, K.Y., Babri, S., Lu, C., Södersten, C.J.H., 2021. A battery electric bus energy consumption model for strategic purposes: validation of a proposed model structure with data from bus fleets in China and Norway. Transp. Res. Part D: Transp. Environ. 94, 102804.

Ho, S.C., Szeto, W.Y., Kuo, Y.-H., Leung, J.M.Y., Petering, M., Tou, T.W.H., 2018. A survey of dial-a-ride problems: literature review and recent developments. Transp. Res. B Methodol. 111, 395–421.

Jansen, M.J.W., 1999. Analysis of variance designs for model output. Comput. Phys. Commun. 117, 35–43.

Jeong, J., Ghaddar, B., Zufferey, N., Nathwani, J., 2024. Adaptive robust electric vehicle routing under energy consumption uncertainty. Transp. Res. Part C Emerging Technol. 160, 104529.

Jiang, J., Yu, Y., Min, H., Cao, Q., Sun, W., Zhang, Z., Luo, C., 2023. Trip-level energy consumption prediction model for electric bus combining Markov-based speed profile generation and Gaussian processing regression. Energy 263, 125866.

Keskin, M., Çatay, B., 2016. Partial recharge strategies for the electric vehicle routing problem with time windows. Transp. Res. Part C Emerging Technol. 65, 111–127.

Koc, C., Karaoglanba, I., 2016. The green vehicle routing problem: a heuristic based exact solution approach. Appl. Soft Comput. 39, 154–164.

Li, W., Wub, G., Zhang, Y., Barth, M.J., 2017. A comparative study on data segregation for mesoscopic energy modeling. Transp. Res. Part D: Transp. Environ. 50, 70–82.

Lian, Y., Lucas, F., Sörensen, K., 2023. The electric on-demand bus routing problem with partial charging and nonlinear function. Transp. Res. Part C Emerging Technol. 157, 104368.

Lu, J., Chen, Y., Hao, J.-K., He, R., 2020. The time-dependent electric vehicle routing problem: model and solution. Expert Syst. Appl. 161, 113593.

Ma, B., Hu, D., Chen, X., Wang, Y., Wu, X., 2021. The vehicle routing problem with speed optimization for shared autonomous electric vehicles service. Comput. Ind. Eng. 161, 107614.

Masmoudi, M.A., Hosny, M., Demir, E., Genikomsakis, K.N., Cheikhrouhou, N., 2018. The dial-a-ride problem with electric vehicles and battery swapping stations. Transp. Res. Part E: Logist. Transp. Rev. 118, 392–420.

Montanino, M., Punzo, V., 2015. Trajectory data reconstruction and simulation-based validation against macroscopic traffic patterns. Transp. Res. B Methodol. 80, 82–106.

Neaimeh, M., Hill, G.A., Hübner, Y., Blythe, P.T., 2013. Routing systems to extend the driving range of electric vehicles. IET Intelligent Transport System 7 (3), 257–370.

Othman, B., De Nunzio, G., Di Domenico, D., Canudas-de-Wit, C., 2019. Ecological traffic management: a review of the modeling and control strategies for improving environmental sustainability of road transportation. Annu. Rev. Control. 48, 292–311.

Pan, Y., Fang, W., Zhang, W., 2023. Development of an energy consumption prediction model for battery electric vehicles in real-world driving: a combined approach of short-trip segment division and deep learning. J. Clean. Prod. 400, 136742.

Papoulis, A., 1984. Probability. Inc Random Variables and Stochastic Processes. McGraw-Hill.

Patella, S.M., Scrucca, F., Asdrubali, F., Carrese, S., 2019. Carbon footprint of autonomous vehicles at the urban mobility system level: a traffic simulation-based approach. Transp. Res. Part D: Transp. Environ. 74, 189–200.

Pelletier, S., Jabali, O., Laporte, G., 2019. The electric vehicle routing problem with energy consumption uncertainty. Transp. Res. B Methodol. 126, 225–255.

Punzo, V., Borzacchiello, M.T., Ciuffo, B., 2011. On the assessment of vehicle trajectory data accuracy and application to the next generation SIMulation (NGSIM) program data. Transp. Res. Part C Emerging Technol. 19 (6), 1243–1262.

Punzo, V., Montanino, M., 2020. A two-level probabilistic approach for robust validation of stochastic traffic simulations: impact of drivers' heterogeneity models. Transp. Res. Part C Emerging Technol. 121, 102843.

Qi, X., Wu, G., Boriboonsomsin, K., Barth, M.B., 2018. Data-driven decomposition analysis and estimation of link-level electric vehicle energy consumption under real-world traffic conditions. Transp. Res. Part D: Transp. Environ. 64, 36–52.
Rakha, H.A., Farag, M., Foroutan, H., 2025. Electric versus gasoline vehicle particulate matter and greenhouse gas emissions: large-scale analysis. Transp. Res. Part D: Trans. Environ. 140, 104622.
Saadon Al-Ogaili, A., Ramasamy, A.K., Hashim, J.T., Al-Masri, A.N., Hoon, Y., Neamah Jebur, M., Verayiah, R., Marsadek, M., 2020. Estimation of the energy consumption of battery driven electric buses by integrating digital elevation and longitudinal dynamic models: Malaysia as a case study. Appl. Energy 280, 115873.
Sagaria, S., Costa Neto, R., Baptista, P., 2021. Assessing the performance of vehicles powered by battery, fuel cell and ultra-capacitor: application to light-duty vehicles and buses. Energ. Conver. Manage. 229, 113767.
Saltelli, A., Ratto, M., Andres, T., Campolongo, F., Cariboni, J., Gatelli, D., Saisana, M., Tarantola, S., 2008. Global Sensitivity Analysis: The Primer. John Wiley & Sons Ltd.
Saltelli, A., Annoni, P., Azzini, I., Campolongo, F., Ratto, M., Tarantola, S., 2010. Variance based sensitivity analysis of model output. design and estimator for the total sensitivity index. Comput. Phys. Commun. 181 (2), 259–270.
Saltelli A., Annoni P., 2010. How to avoid a perfunctory sensitivity analysis. Environmental Modelling and Software, 25 (12), 1508 - 1517.
Saltelli, A., Bammer, G., Bruno, I., Charters, E., Di Fiore, M., Didier, E., Espeland, W.N., Kay, J., Lo, P.S., Mayo, D., Pielke Jr., R., Portaluri, T., Porter, T.M., Puy, A., Rafols, I., Ravetz, J.R., Reinert, E., Sarewitz, D., Stark, P.B., Stirling, A., van der Sluijs, J., Vineis, P., 2020. Five ways to ensure that models serve society: a manifesto. Nature 582 (7813), 482–484.
Sayarshad, H.R., Mahmoodian, V., Gao, H.O., 2020. Non-myopic dynamic routing of electric taxis with battery swapping stations. Sustain. Cities Soc. 57, 102113.
Schiffer, M., Walther, G., 2017. The electric location routing problem with time windows and partial recharging. Eur. J. Oper. Res. 260 (3), 995–1013.
Schneider, M., Stenger, A., Goeke, D., 2014. The electric vehicle-routing problem with time windows and recharging stations. Transp. Sci. 48 (4), 500–520.
Shankar, R., Marco, J., 2013. Method for estimating the energy consumption of electric vehicles and plug-in hybrid electric vehicles under real-world driving conditions. IET Intell. Trans. Syst. 7 (1), 138–150.
Sobol, I.M., 1967. Distribution of points in a cube and approximate evaluation of integrals. U.S.S.R comput. Maths. Math. Phys. 7, 86–112.
Sobol, I.M., 2001. Global sensitivity indices for nonlinear mathematical models and their Monte Carlo estimates. Math. Comput. Simul. 55, 271–280.
Su, Y., Dupin, N., Puchinger, J., 2023. A deterministic annealing local search for the electric autonomous dial-a-ride problem. Eur. J. Oper. Res. 309 (3), 1091–1111.
Wang, X., Jiang, J., Zhou, Y., Wang, X., 2023. Integrated infrastructure planning of charging and electricity generation. Transp. Res. Part D: Transp. Environ. 122, 103807.
Wang, Y., Huang, Y., Xu, J., Barclay, N., 2017. Optimal recharging scheduling for urban electric buses: a case study in Davis. Transp. Res. Part E: Logist. Transp. Rev. 100, 115–132.
Wen, M., Linde, E., Ropke, S., Mirchandani, P., Larsenet, A., 2016. An adaptive large neighborhood search heuristic for the electric vehicle scheduling problem. Comput. Oper. Res. 76, 73–83.
Wu, X., Freese, D., Cabrera, A., Kitch, W.A., 2015. Electric vehicles' energy consumption measurement and estimation. Transp. Res. Part D: Transp. Environ. 34, 52–67.
Xu, H., Tu, R., Li, T., Chen, H., 2023. Interpretable bus energy consumption model with minimal input variables considering powertrain types. Transp. Res. Part D: Transp. Environ. 119, 103742.
Yao, E., Wang, M., Song, Y., Zhang, Y., 2014. Estimating energy consumption on the basis of microscopic driving parameters for electric vehicles. Transp. Res. Rec. 2454 (1), 84–91.
Yi, Z., Bauer, P.H., 2017. Adaptive multiresolution energy consumption prediction for electric vehicles. IEEE Trans. Veh. Technol. 66 (11), 10515–10525, 7961181.
Yi, Z., Smart, J., Shirk, M., 2018. Energy impact evaluation for eco-routing and charging of autonomous electric vehicle fleet: ambient temperature consideration. Transp. Res. Part C Emerging Technol. 89, 344–363.
Yousefi, G., Dimovski, A., Radaelli, L., Merlo, M., 2024. Estimating the impact of electric mobility on distribution networks through GIS techniques. Sustainable Energy Grids Networks 38, 101379.
Zhang, J., Wang, Z., Liu, P., Zhang, Z., 2020. Energy consumption analysis and prediction of electric vehicles based on real-world driving data. Appl. Energy 275, 115408.
Zhang, R., Yao, E., 2015. Electric vehicles' energy consumption estimation with real driving condition data. Transp. Res. Part D: Transp. Environ. 41, 177–187.
Zhang, S., Gajpal, Y., Appadoo, S.S., Abdulkader, M.M.S., 2018. Electric vehicle routing problem with recharging stations for minimizing energy consumption. Int. J. Prod. Econ. 203, 404–413.
Zhuge, C., Shao, C., Yang, X., 2019. Agent- and activity-based large-scale simulation of enroute travel, enroute refuelling and parking behaviours in Beijing. China. J. Comput. Sci. 38, 101046.